Towards Systems Behavior Factors for Composite Frames: Experimental and Analytical Studies

A Summary Final Report to the
American Institute of Steel Construction

by

Roberto T. Leon and Tiziano Perea
School of Civil and Environmental Engineering
Georgia Tech, Atlanta, GA

Jerome F. Hajjar
Department of Civil and Environmental Engineering
Northeastern University, Boston, MA

Mark D. Denavit
Department of Civil and Environmental Engineering
University of Illinois at Urbana-Champaign, Urbana, IL

February 2011

I. Introduction

Composite steel-concrete structural systems constitute a valuable and growing sector of the construction market, often being adopted for some of the more challenging construction configurations because of the high strength and stiffness offered by these systems. At the present time, it remains difficult to predict the maximum structural response of a frame system that includes composite beam-columns based on typical frame analysis and design strategies. Fiber Analysis (FA) or Finite Element Analysis (FEA) may be used to obtain an improved assessment of the response; however, their application in conventional design of low- to moderate- height buildings is neither practical nor common. The development of stability design procedures and seismic design parameters or behavior factors applicable solely to composite systems incorporating steel reinforced concrete (SRC) or concrete-filled steel tube (CFT) columns, as opposed to using those for similar steel or RC structural systems, is also needed. To reach these goals, a multi-institution combined experimental/computational research program was undertaken, including: (a) experiments of slender, full-scale concrete-filled steel tube beam-columns that included slender cross-sections to fill the gaps in the experimental databases; (b) development of new finite element formulations that enable accurate representation of the seismic response of three-dimensional composite braced and unbraced frame structures; and, (c) recommendations for design of composite structures within the context of the American Institute of Steel Construction *Specification for Structural Steel Buildings*, including interaction effects, effective rigidities, bond provisions, construction considerations, and analysis recommendations. This work serves as the foundation for the second part of the study, in which a large number of nonlinear dynamic analyses have been carried out to evaluate the performance of this system and to develop the system behavior factors.

The main objectives of the experimental component of this research are:

- To obtain experimentally the critical load of slender composite circular CFT (CCFT) and rectangular CFT (RCFT) full-scale beam-columns with different boundary conditions. There is a dearth of data on slender composite columns and the possible interaction between the stability and strength of the section, as well as the ability of slender CFT cross sections to confine the concrete.

- To obtain experimentally a large number of data points on or near the axial load-moment (*P-M*) interaction diagram of composite CFT beam-columns. There is very little data on the ultimate strength of composite sections under different combinations of axial load and moment, particularly when coupled with large lateral deformations and three-dimensional loading.

- To obtain experimental response of CFT beam-columns under cyclic lateral forces, and from this, evaluate the strength and ductility of slender CFT beam-columns for seismic loading. In addition, this research provides some of the most detailed data in the literature regarding the evolution of stiffness, strength, and damage in composite members.

- To evaluate the effect of the wet concrete in steel tubes during the pouring, while acting under hydrostatic pressure, while in the transition to a hardening state, and when the element is loaded compositely during the experiments.

- To evaluate the effects of the stability, concrete confinement, steel local buckling, and the interrelation among these on the behavior of CFTs.

- To refine material constitutive models and structural models to have an analytical prediction that follows the experimental response.

- To provide recommendations for the construction and the design of circular and rectangular composite CFT beam-columns in frame structures.

The main objectives of the analytical component of this research are:

- To develop a comprehensive set of experimental data from the worldwide literature on SRC and CFT composite members and frames.

- To formulate and validate advanced nonlinear models for the analysis of steel and concrete composite frames through the development of distributed plasticity fiber-based beam finite element formulations.

- To provide recommendations for the assessment of load transfer via natural bond strength for rectangular and circular CFT columns.

- To design a series of archetype frames suitable for the parametric studies to establish seismic response factors, direct analysis parameters for stability design, and to provide related analysis/design recommendations.

The purpose of this report is to provide brief highlights of the research. Complete details of this research are reported in Leon *et al.* (2009), Denavit and Hajjar (2010), Denavit *et al.* (2010), Perea *et al.* (2010) and Perea (2010). Together these reports summarize the prior literature on experimental testing of composite beam-columns, computational formulations for composite construction, and behavioral assessment of composite members. The reports also present a comprehensive set of data obtained from the experimental program, detailed analysis of experimental results, and a complete description of the formulation and validation of the computational model.

II. *Experimental Methodology*

The experimental program consisted in testing 18 full-scale concrete-filled steel tube beam-columns subjected to complex three-dimensional load protocols. These complex full-scale tests were possible due to the capabilities of the Multi-Axial Sub-assemblage Testing laboratory (MAST), a part of the NEES Collaboratory (Hajjar *et al.* 2002). At the time this program was conducted, these CFT specimens were the slenderest and the longest CFT columns and beam-columns tested in the world.

Tests Specimens

The test matrix is summarized in Table 1. An extensive database (Leon *et al.* 2005, Goode 2007) was used to identify gaps in existing knowledge; these gaps were particularly clear for very slender columns and for beam-columns with high-strength concrete. Thus the test matrix consists of a mix of three circular CFT and one rectangular CFT specimens with lengths of 18 ft.

and 26 ft. and concrete infills with nominal strengths of 5 ksi and 12 ksi. The rectangular CFTs were tested both in their strong (s) and weak (w) axis directions. Specimens with the most slender walls commonly available were used. Typical details of these specimens are shown in Figures 1 through 4.

Table 1 – Test matrix of the CFT specimens with nominal values

Specimen name	L (ft)	Steel section HSS D x t	F_y (ksi)	f_c' (ksi)	D/t
C5-18-5	18	HSS5.563x0.134	42	5	45
C12-18-5	18	HSS12.75X0.25	42	5	55
C20-18-5	18	HSS20x0.25	42	5	86
Rw-18-5	18	HSS20x12x0.25	46	5	67
Rs-18-5	18	HSS20x12x0.25	46	5	67
C12-18-12	18	HSS12.75X0.25	42	12	55
C20-18-12	18	HSS20x0.25	42	12	86
Rw-18-12	18	HSS20x12x0.25	46	12	67
Rs-18-12	18	HSS20x12x0.25	46	12	67
C12-26-5	26	HSS12.75X0.25	42	5	55
C20-26-5	26	HSS20x0.25	42	5	86
Rw-26-5	26	HSS20x12x0.25	46	5	67
Rs-26-5	26	HSS20x12x0.25	46	5	67
C12-26-12	26	HSS12.75X0.25	42	12	55
C20-26-12	26	HSS20x0.25	42	12	86
Rw-26-12	26	HSS20x12x0.25	46	12	67
Rs-26-12	26	HSS20x12x0.25	46	12	67
C5-26-12	26	HSS5.563x0.134	42	12	45
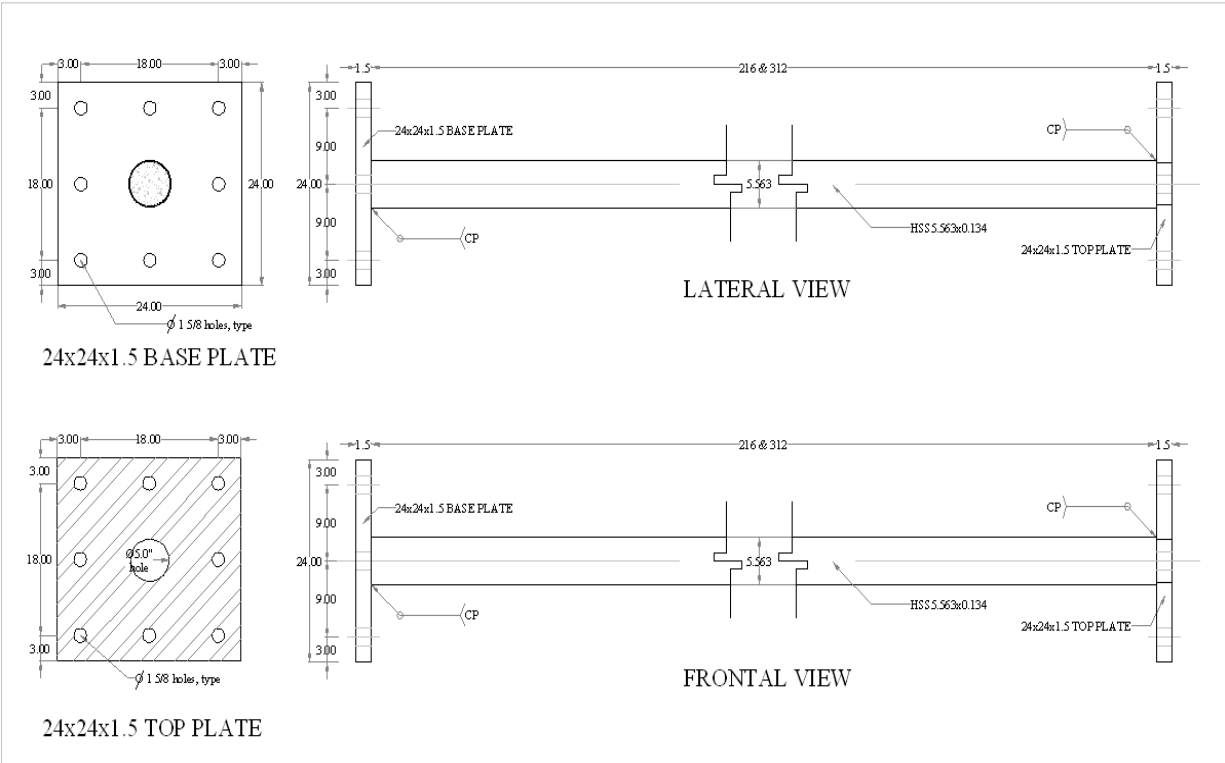
Figure 1 – Circular CFT specimen with an HSS5.563x0.134
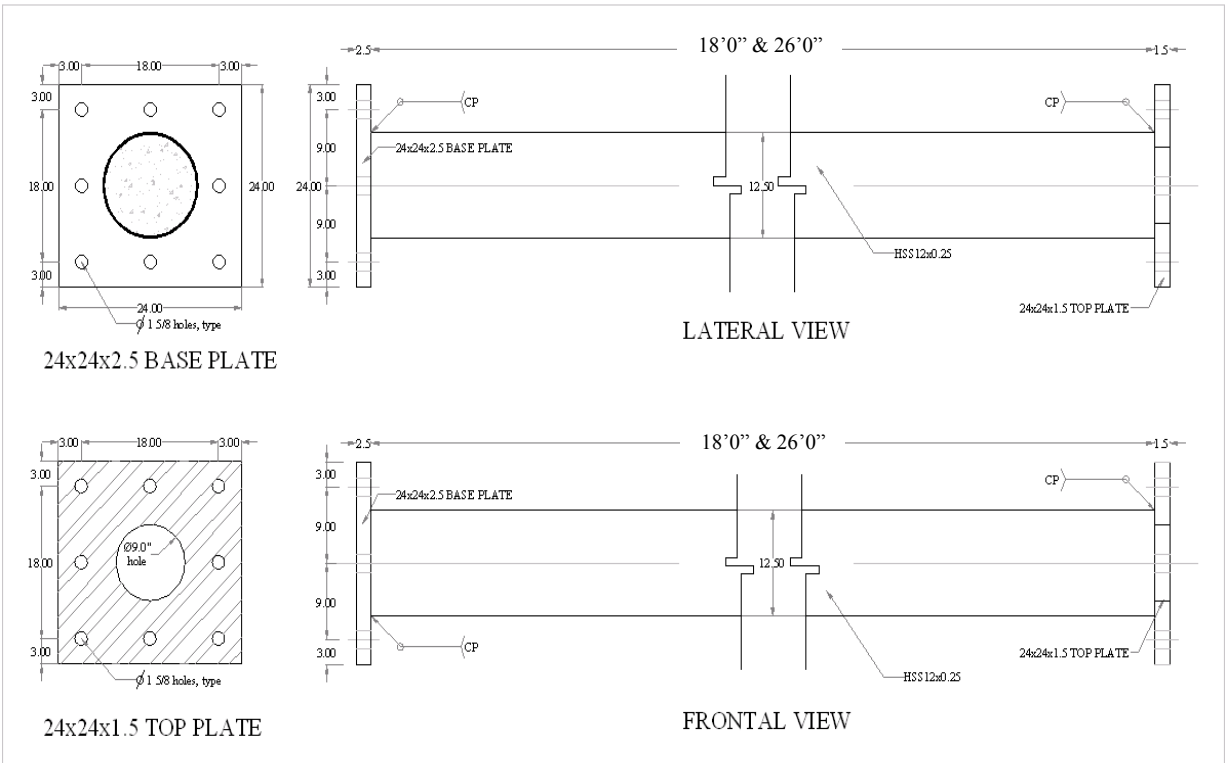
Figure 2 – Circular CFT specimen with an HSS12.75x0.25
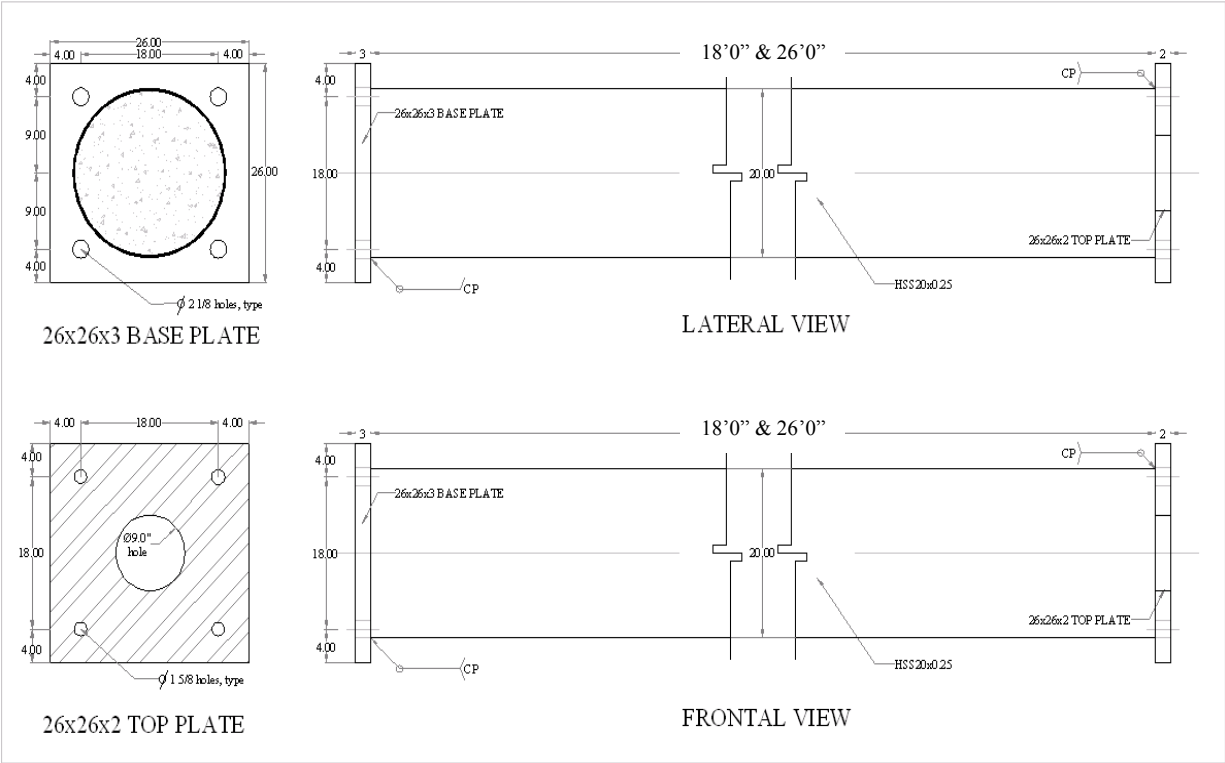
Figure 3 – Circular CFT specimen with an HSS20x0.25
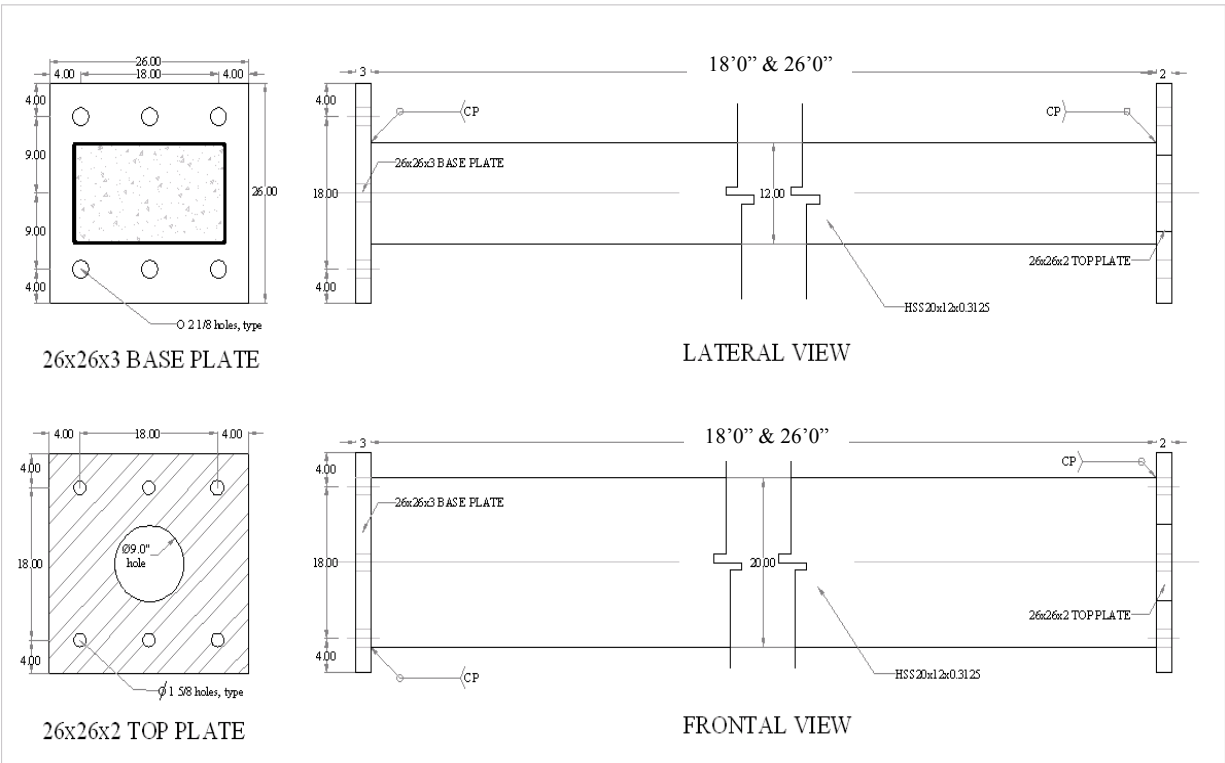
Figure 4 – Rectangular CFT specimen with an HSS20x12x0.3125

III. Instrumentation Plan

The instrumentation of the specimens consisted of:

- Strain gages for measuring both longitudinal and transverse strains. The strain gages were placed in three (and in some cases four) faces of the exterior steel wall. At least three measurements at the same level of the column allow the complete calculation of strain within the cross-section assuming plane sections remain plane.

- LVDTs for measuring relative displacements (elongation of shortening) along the specimen. As with the strain gages, LVDTs were placed on three faces to allow the calculation of the relative displacement at any point within the cross-section assuming plane sections remain plane. LVDTs were attached to the specimen through a set of brackets bolted and studs welded to the steel.

- String-pots for measuring lateral displacements and getting the displaced profile in both horizontal axes.

- LEDs for measuring the position change of a set of points. These measurements are captured by the Krypton system (Metris K600 Dynamic Measuring Machine, DMM), which measured detailed three-dimensional position of the target points placed on the specimen..

Additional calculated channels were obtained from the measured data. Some of these calculations include, but are not limited to:

- Moments at the base, and at different points along the specimen

- Rotations and curvatures at different cross-sections

- Evolution of the displaced shape or deformation in some segments.

- Stresses at different positions through the cross-section and the specimen length.

IV. Loading Histories

The Multi-Axial Sub-assemblage Testing (MAST) system, as shown in Figure 5, consists of a stiff steel crosshead connected to 4 vertical actuators (each with a capacity of 330 kips and ±20 in. strokes) and 2 actuators in each horizontal axis (each with a capacity of 440 kips and ±16 in. strokes). The MAST system has the capability of controlling the 6 DOFs independently with a maximum capacity of P_z = 1320 kips of vertical force and $V_x=V_y=880$ kips of horizontal force.

The MAST facility has permitted the use of very complex load histories, which were needed for the calibration of the analysis models and to validate complex behavior of composite beam-columns. Each test consisted of several load cases, with each case having one or more cycles. A typical set of load cycles is shown in Table 2. Load case 0 was used to get rid of forces and moments induced during the specimen-crosshead connection and adjust the initial position of the specimen to account for initial imperfections, a key factor in the stability study. Load case 1 consisted of a buckling test with the column subjected to axial load and idealized as pinned-free, as shown in Figure 6. Load case 2 consisted of applying an axial load, followed by a series of

uniaxial lateral displacements. Load case 3 is similar to load case 2, but the displacements are biaxial. Local case 4 corresponds to torsional loading.

Figure 7 shows typical results for load case 1, with forces measured from the loads cells in the testing machine. For comparison, the cross-sectional strength and a simplified *P-M* interaction diagram including length effects are also shown.

As an example of the complexity of the possible load histories, Figure 8 shows a combination of Load Cases 2 and 3, in which the deformations in the X and Y directions were imposed while maintaining the moments at the top at zero. The graphs show the moments at the bottom as given by equilibrium calculations from external loads. Load case 2 is a uniaxial bending case, while case 3 is a biaxial case. In load case 3, the resulting moment at the bottom are affected by the initial imperfections, resulting in the spiral patterns shown.
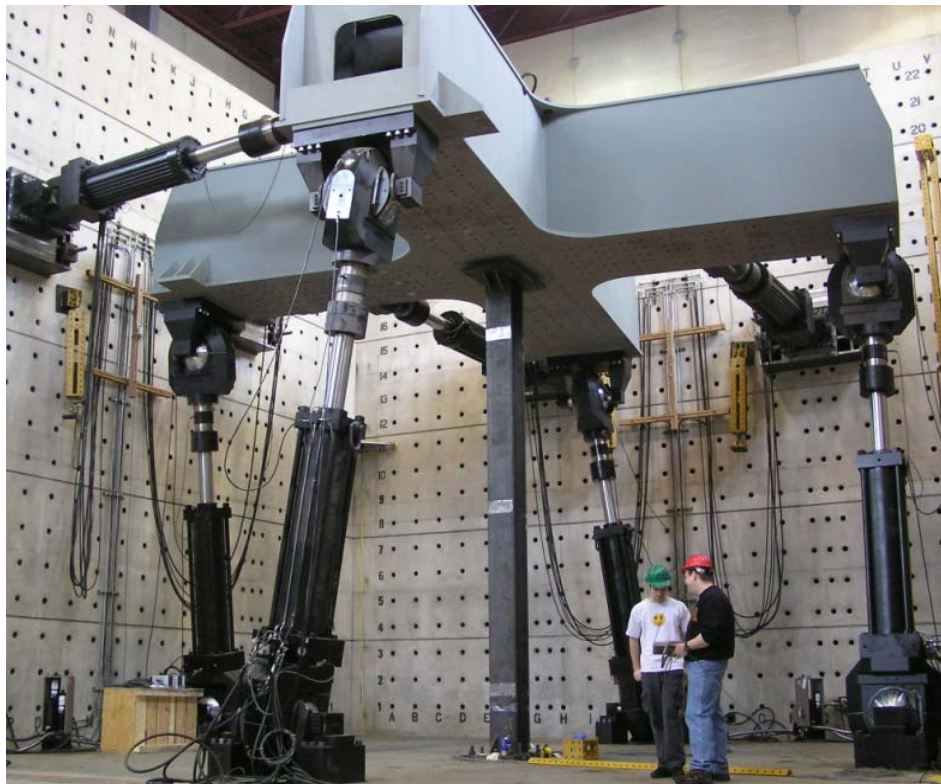
Figure 5 – Overall view of MAST facility.
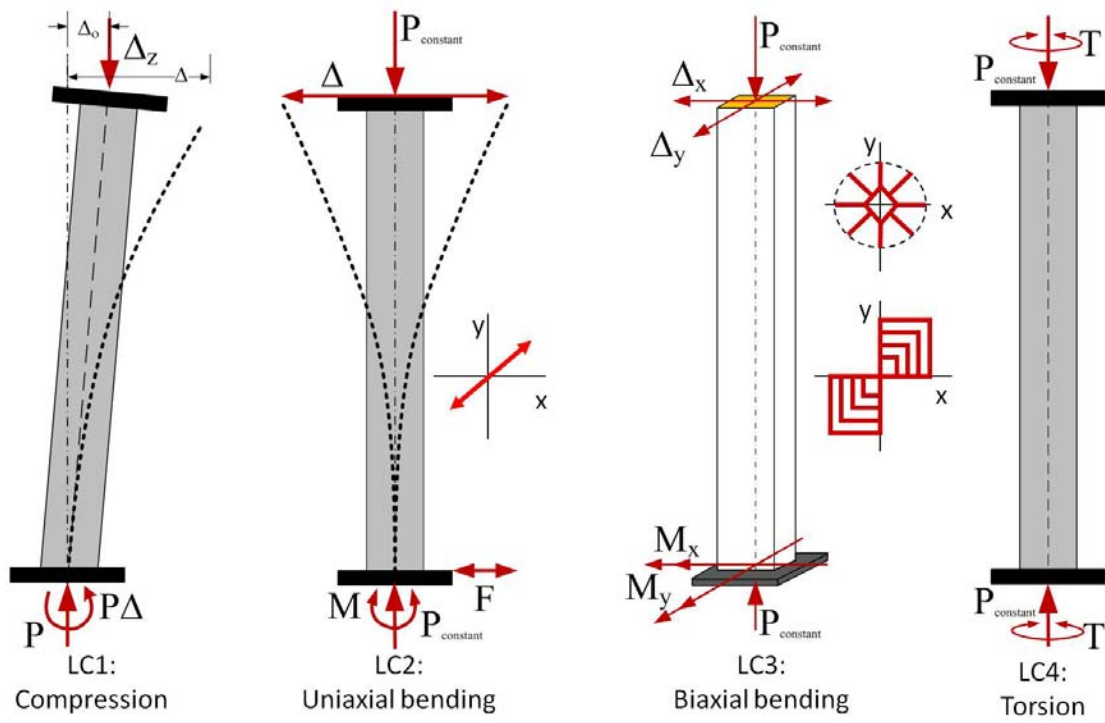
Figure 6 – Load histories.

Table 2 – Typical Load History

Load Case	Step	Action	Degree of Freedom					
			Δ_x/F_x	Δ_y/F_y	Δ_z/F_z	R_x/M_x	R_y/M_y	R_z/M_z
0	1	Set zeros	$F_x = 0$	$F_y = 0$	$F_z = 0$ $\Delta_z = 0$	$M_x = 0$ $R_x = 0$	$M_y = 0$ $R_y = 0$	$M_z = 0$ $R_z = 0$
	2	Adjustment $\Delta_y = 0$	$F_x = 0$	Δ_y controlled	$F_z = 0$	$M_x = 0$	$M_y = 0$	$R_z = 0$
1a	1	Concentric Loading	$F_x = 0$	$\Delta_y = 0$	Δ_z controlled	$M_x = 0$	$M_y = 0$	$R_z = 0$
	2	Concentric Unloading	$F_x = 0$	$\Delta_y = 0$	Δ_z controlled	$M_x = 0$	$M_y = 0$	$R_z = 0$
2a	1	Uniaxial Loading	Δ_x controlled	$\Delta_y = 0$	$F_z = 0.50\ P_C$	$M_x = 0$	$M_y = 0$	$R_z = 0$
2b	1	Uniaxial Loading	Δ_x controlled	$\Delta_y = 0$	$F_z = 1.00\ P_C$	$M_x = 0$	$M_y = 0$	$R_z = 0$
3a	1	Biaxial Loading	Δ_x & Δ_y controlled		$F_z = 0.25\ P_C$	$M_x = 0$	$M_y = 0$	$R_z = 0$
3b	1	Biaxial Loading	(diagram: y–x axes with radial loading directions)		$F_z = 0.75\ P_C$	$M_x = 0$	$M_y = 0$	$R_z = 0$
3c	1	Biaxial Loading			$F_z = 1.50\ P_C$	$M_x = 0$	$M_y = 0$	$R_z = 0$
4a	1	Pure Torsion	$\Delta_x = 0$	$\Delta_y = 0$	$F_z = 0$	$M_x = 0$	$M_y = 0$	Δ_z controlled
	2	Torsion & axial load	$\Delta_x = 0$	$\Delta_y = 0$	$F_z = 0.2\ P_o$	$M_x = 0$	$M_y = 0$	Δ_z controlled
4b	1	Concentric Loading	$\Delta_x = 0$	$\Delta_y = 0$	Δ_z controlled	$M_x = 0$	$M_y = 0$	$R_z = 0$
	2	Biaxial Loading	Δ_x & Δ_y controlled (diagram: y–x axes with diagonal loading)		$F_z = 1.50\ P_C$	$M_x = 0$	$M_y = 0$	$R_z = 0$
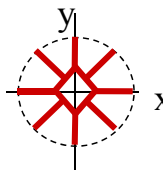
(a) Specimen 4-Rw-18-5   (b) Specimen 8- Rw-18-12
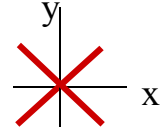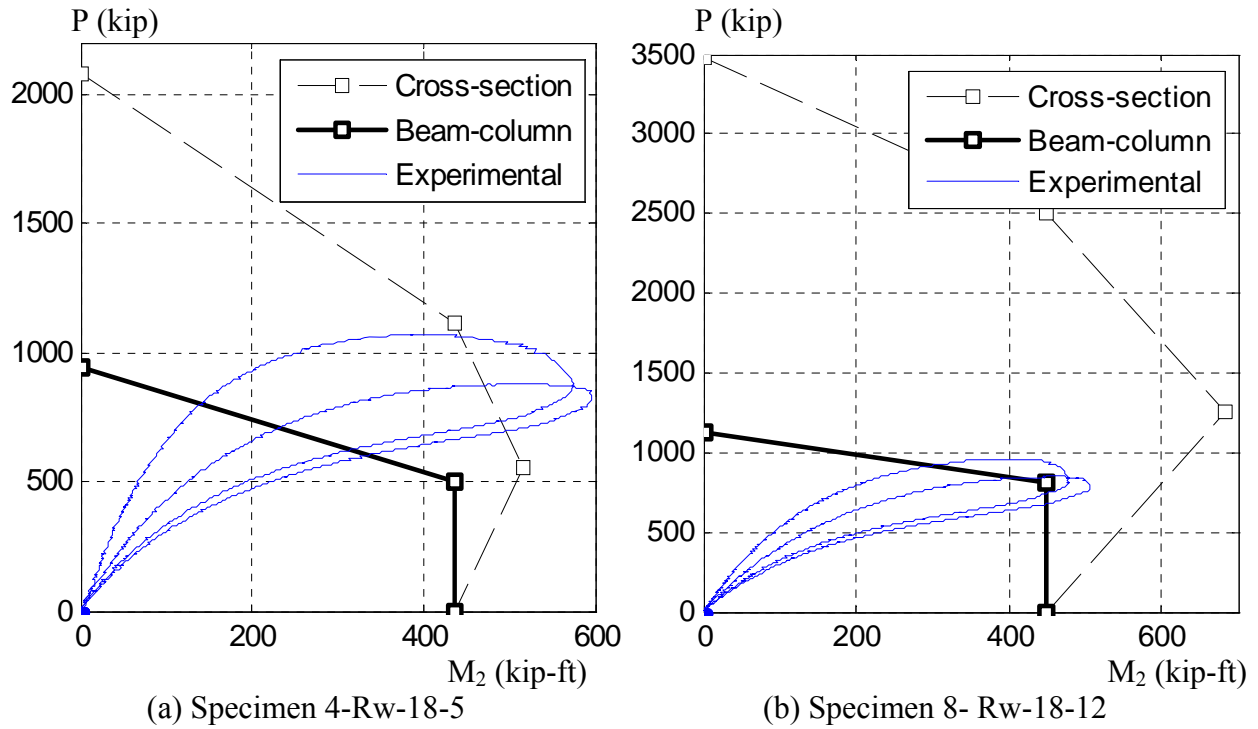
Figure 7 – Typical results of buckling test with moments based on crosshead forces
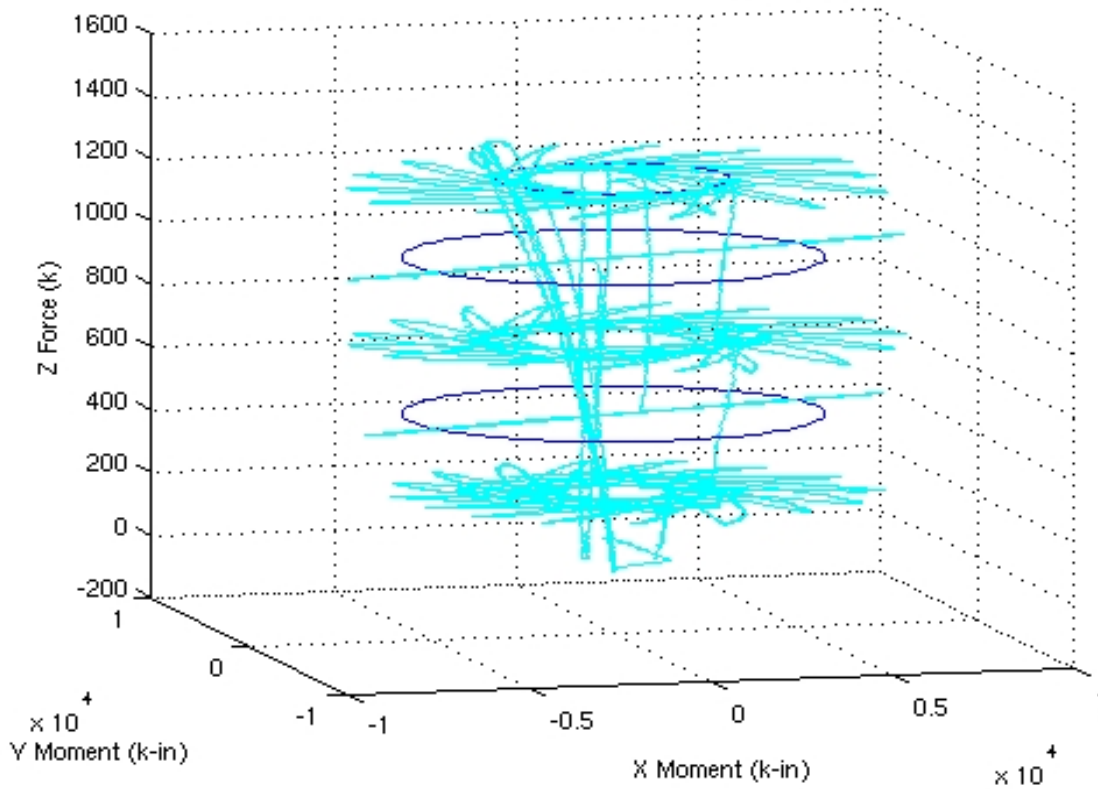
Figure 8 – Load cases 2 (uniaxial bending at three axial load levels show by circles)
and 3 (biaxial bending at three load levels)

V. *Experimental Results*

Wet Concrete

Since this research intended to test very long CFT specimens, initial deformations on the steel tubes induced by the concrete during casting were considered in advance of the construction process and the data analysis. The stresses and deformations in the steel tube under hydrostatic pressure were evaluated with closed-form analytical solutions and complemented with finite element analysis. These analytical results indicated that problems would arise in the RCFT specimens, unless stresses and deformations were limited to reasonable values. For this reason, stiffeners were used during casting of most of the RCFT specimens to control the initial deformations due to the hydrostatic pressure of wet concrete. During the testing of the RCFTs, adverse effects were clear in those specimens that were not stiffened, as the testing started with considerable initial outward deformations on the plates. These deformations led to an earlier initiation of the steel local buckling at the elevation where the maximum outward deflection initially occurred as a consequence of the wet concrete pressure. In contrast, there were very low initial deformations on the plates of those specimens that were stiffened properly, and in these cases the local buckling developed as expected at the critical section (near the base) and only as a consequence of interaction of high strains and the slender walls.

Recommendations to minimize the effects of the wet concrete pressures include simplified equations to estimate the maximum transverse stress and the maximum outward expansion that may occur in a RCFT member at the casting process. The limits are:

$$\sigma_{max} = \max \left[\begin{array}{c} \left(\dfrac{2h_c}{b_c + 4h_c} \right) \dfrac{p \cdot h_c^2}{t^2} \\[2ex] \dfrac{1}{3} \left(\dfrac{3b_c + 4h_c}{b_c + 4h_c} \right) \dfrac{p \cdot h_c^2}{t^2} \end{array} \right] \leq \dfrac{F_y}{\Omega} \tag{1}$$

$$\delta_{max} = \dfrac{1}{32} \left(\dfrac{5b_c + 4h_c}{b_c + 4h_c} \right) \dfrac{p \cdot h_c^4}{E_s \cdot t^3} \leq \dfrac{L}{2000} \tag{2}$$

where, h_c and b_c are, respectively, the longer and the shorter inner widths of the rectangular cross-section ($h_c = h - 2t$; $b_c = b - 2t$), t is the thickness, b and h are the overall outside dimensions, L is the pressure length, and p is the hydrostatic pressure. If either the corresponding stresses or deformations in rectangular CFT cross sections exceed the limits above, it is recommended that external supports be added during casting. Member strength may then be assessed using current procedures.

Buckling Tests

Results for Load Case 1 are shown, in their uncorrected form, in Figure 9. In Table 3, the P_n values are computed following the 2010 AISC Specification, but using actual material values and imperfections, $K=2$, and no resistance factors. It should be noted that several tests (open symbols), did not achieve the expected buckling loads due to lack of axial load capacity. For a correct assessment of the data, these results needed to be corrected for the following reasons:

- In several cases, as the true buckling load was approached, the horizontal forces at the top of the column, which theoretically should be zero, began to increase and thus $K<2$.
- The test controller did not take into account the compliance of the loading system.
- The clevis pins in the actuators contributed some frictional forces.
- The initial imperfections were different from those assumed in the AISC design equations.

The corrected data is shown in both Figure 10 and Table 3. Overall, the results show very good correlation to the expected values, indicating that the current AISC design procedures are accurate for slender sections and that the effect of confinement decreases as the slenderness increases.

Table 3 – Load Case 1 results

Specimen	f_c (ksi)	F_y (ksi)	L (ft, in)	Δ_o/L (%)	δ_o/L (%)	K -	λ -	P_n (kip)	P_{exp} (kip)
1C5-18-5	5.5	55.6	18' $^1/_2$"	0.000	0.711*	0.5	0.90	166	129
18C5-26-12	11.7	55.6	26' $^5/_8$"	0.000	0.196*	0.5	1.51	140	141
2C12-18-5	5.6	48.9	18' $^1/_2$"	0.376	0.035	2	1.55	393	400
6C12-18-12	13.2	48.9	18' $^1/_2$"	0.197	0.049	2	1.90	472	500
10C12-26-5	7.9	48.6	26' 1"	0.322	0.020	2	2.38	207	222
14C12-26-12	11.6	55.5	26' $1^1/_2$"	0.213	0.023	2	2.72	216	225
3C20-18-5	5.8	47.6	18' $1^1/_2$"	0.438	0.084	2	1.05	1469	1478
7C20-18-12	13.2	47.6	18' $1^7/_8$"	0.449	0.039	2	1.30	2190	1791
11C20-26-5	8.1	44.3	26' $2^3/_4$"	0.700	0.121	2	1.61	992	802
15C20-26-12	11.6	42.5	26' 2"	0.522	0.076	2	1.78	1080	1100
4Rw-18-5	5.9	53.0	18' 2"	0.615	0.029	2	1.38	939	950
8Rw-18-12	13.3	53.0	18' $2^5/_8$"	0.828	0.010	2	1.65	1124	961
12Rw-26-5	8.2	58.9	26' $1^1/_4$"	0.084	0.084	2	2.14	501	540
16Rw-26-12	11.7	55.2	26' $1^1/_4$"	0.193	0.100	2	2.30	534	673
5Rs-18-5	5.9	53.0	18' 2"	0.037	0.036	2	0.88	1501	1521
9Rs-18-12	13.3	53.0	18' $2^5/_8$"	0.360	0.036	2	1.04	2209	1918
13Rs-26-5	8.3	55.5	26' $1^3/_4$"	0.216	0.030	2	1.35	1199	1200
17Rs-26-12	11.7	55.1	26' $1^1/_2$"	0.523	0.019	2	1.46	1323	1120

(*) The values stated in this table correspond to the out-of-straightness at the beginning of the load case. The initial out-of-straightness (δ_o/L) before testing were 0.045% and 0.074% for the specimens 1 and 18, respectively.
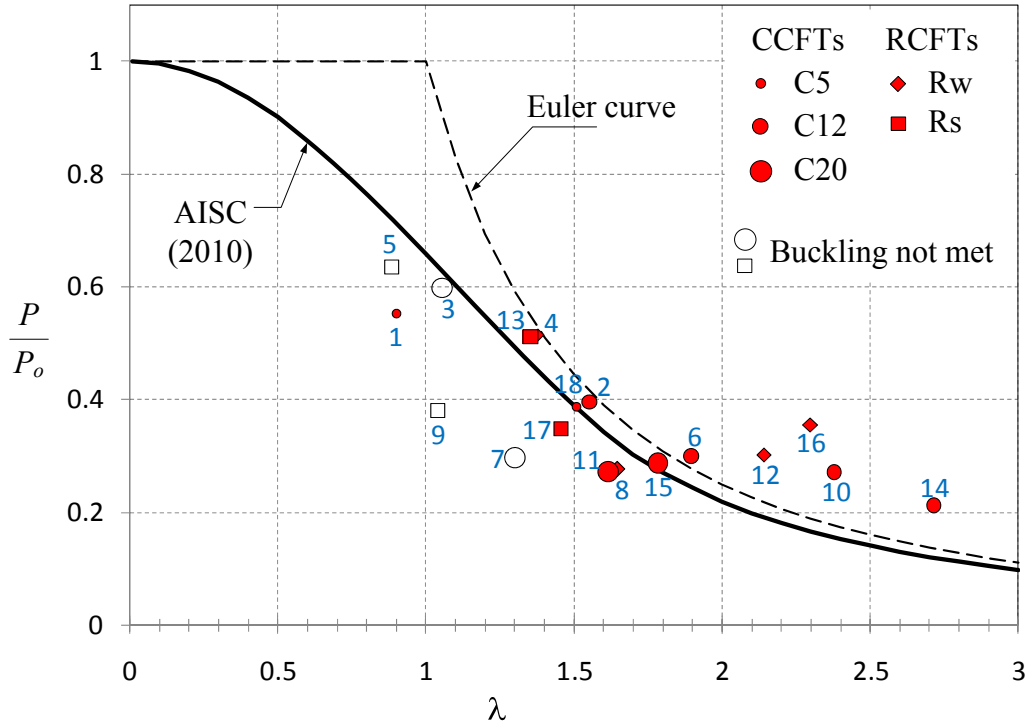
Figure 9 – Uncorrected data for buckling loads.
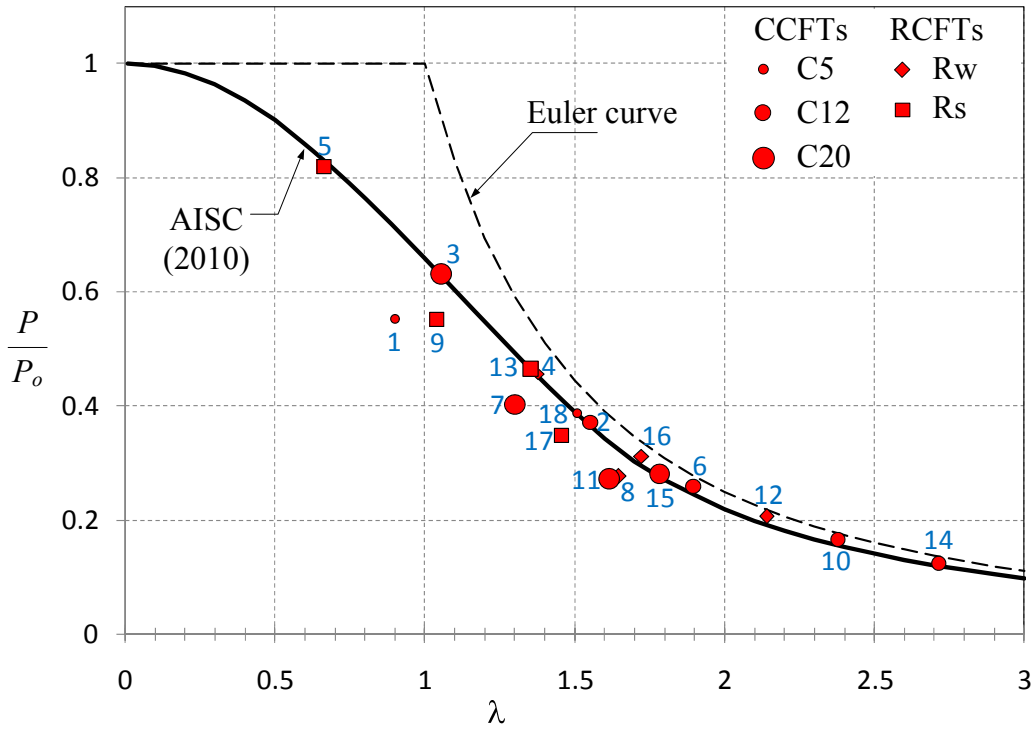
Figure 10 – Corrected data for buckling loads.

Interaction diagrams

To develop interaction (P-M) surfaces, loading cases LC2 and LC3 were used. These load cases consisted of a constant compression force in load control, while the top is driven laterally in displacement control (Figure 11(a)). The methodology used for the extraction of experimental P-M values of interaction has been previously used for the calibration of the interaction equations for steel members in the AISC Specifications and Eurocodes, using data obtained from second-order inelastic analysis of benchmark steel frames. The maximum stable capacity of a beam column is defined by its maximum lateral strength (F_{max}) at which the incipient instability condition arises (Figure 11(b)). The total second order moment consists of the first order moment (FL) and the second order moments (P-Δ), as shown in Figure 11(c). Beyond F_{max}, the beam-column is in an unstable condition even when the critical cross-section still has some remaining capacity. A set of axial load (P) and base moment (M) points related to the instant when the specimen reached the maximum stable capacity (F_{max}) are extracted and compiled as the *total beam-column capacity*. The total capacity as defined above does not incorporate the effects of the initial imperfections. Initial imperfections tend to increase the demands from second-order effects, and as a result, the available first-order moment capacity is reduced. The initial imperfections can be included as the difference between the total capacity and that capacity consumed by the imperfections. The resultant P-M points from the previous process are compiled as the *net beam-column capacity*. The experimental results included in Figure 10(d) include: (a) the pure compression loading (LC1) up to a given level of gravity force (cyan line and square); (b) the path from the uniaxial bending loading (LC2) up to a total second order moment at incipient buckling (M_{total}, blank square); and (c) the net second-order moment (M_{net}, black square).
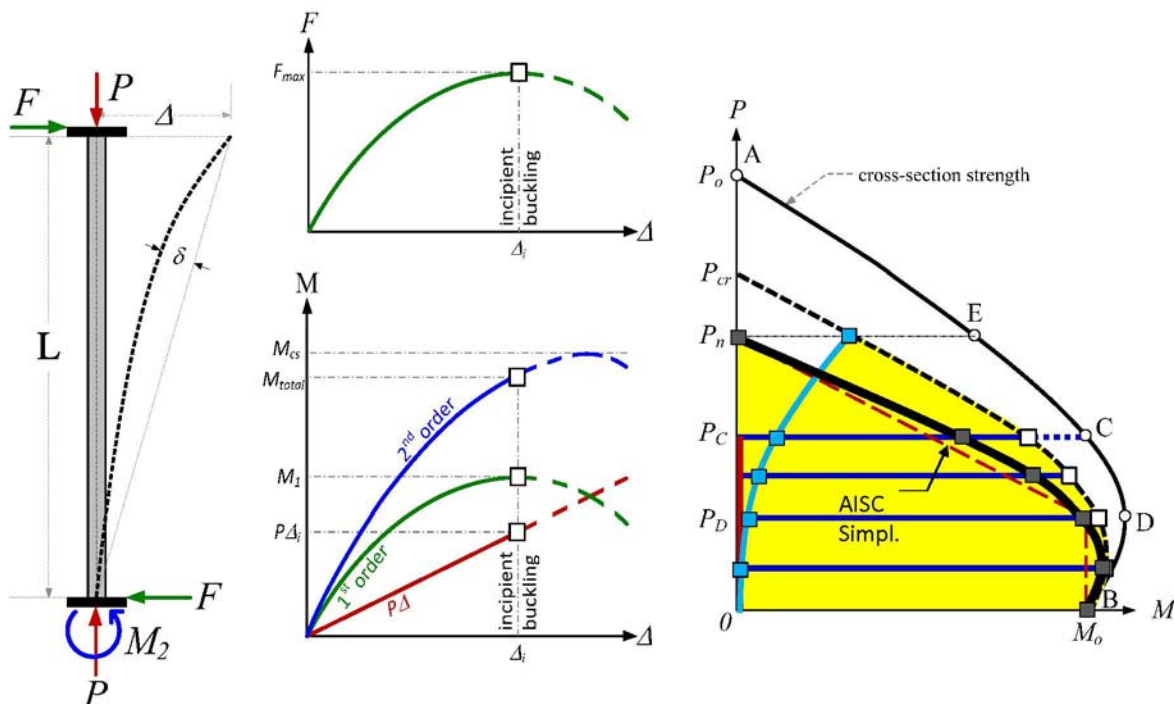
Figure 11 – Extraction of P-M interaction values from experimental data

The net moments extracted from the test specimens are then compared with the simplified interaction diagram proposed in the AISC (2010) Specifications for composite beam-columns. The following observations were noted from these comparisons (Figure 12):

- In the shorter specimens, the net *P-M* capacities extracted from the tests drop outside of the bilinear simplified diagram of the AISC for beam-columns, which underestimates the *P-M* capacities of the shorter specimens around the points C_λ-*B*. The purpose of neglecting the bulge with this vertical line in the AISC Simplified diagram intended to be conservative through a lower bound, and this simplification was supported by the available experimental data at the time.
- The shape of the bilinear simplified diagram turned out to be less conservative in beam-columns with intermediate slenderness; however, for beam-columns with high slenderness, the AISC simplified diagram was unconservative with overestimated net capacities.

It must be noted that the net moment capacities obtained from the experiments has a substantial amount of flexural strength lost due to the large imperfections. Nevertheless, many of these points are still unconservative even if the imperfections are neglected. This unconservative behavior in slender beam-columns suggests a change in the design equations for the calculation of *P-M* interaction diagrams that serves both short and slender beam columns. Similar conclusions were observed in both uniaxial and biaxial bending, as well as in the computational analyses. New proposed equations to eliminate this problem are given in a later section.

Flexural Rigidity for CFT Members

Little well-documented data is available on the effective moment of inertia for composite members. In the current AISC Specification, the effective stiffness is given as:

$$EI_{eff} = E_s I_s + C_3 E_c I_c \qquad \begin{cases} C_3 = 0.1 + 2\left(\dfrac{A_s}{A_s + A_c}\right) < 0.3 & \text{for SRC} \\[2em] C_3 = 0.6 + 2\left(\dfrac{A_s}{A_s + A_c}\right) < 0.9 & \text{for CFT} \end{cases} \qquad \text{(3)}$$

The evaluation of the flexural rigidities extracted from the test results during the entire load protocol exhibited some variability, mainly as the damage in the concrete core and the steel tubes progressed through the load protocol. Figure 12 shows the two main methods used to extract EI values: (a) from the moment-curvature data computed from strain gages, and (b) from load-deflection data. In both cases the values are taken at the beginning of the unloading process. Although dispersion was large, interesting results were extracted from the analysis of this data. A brief summary of the observations includes:

- The averaged values of the flexural rigidities extracted from the response during the pure compression loading case (LC1) were very close to the values predicted by the AISC (2005, 2010) Specifications. However, for the slender sections in this work, the averaged values do not show proportionality with the steel ratio in the cross section (i.e., $\rho = A_s/A$), as indicated by the C_3 coefficient in the equations.

(a) Normalized P-M interaction diagram

(b) Slenderness vs. the normalized net moment

(c) Shorter specimens (λ<1.7)

(d) Slender specimens (λ>1.7)

(e) $M_{net}/M_{AISC} \leq 1.0$

(f) $M_{net}/M_{AISC} > 1.0$
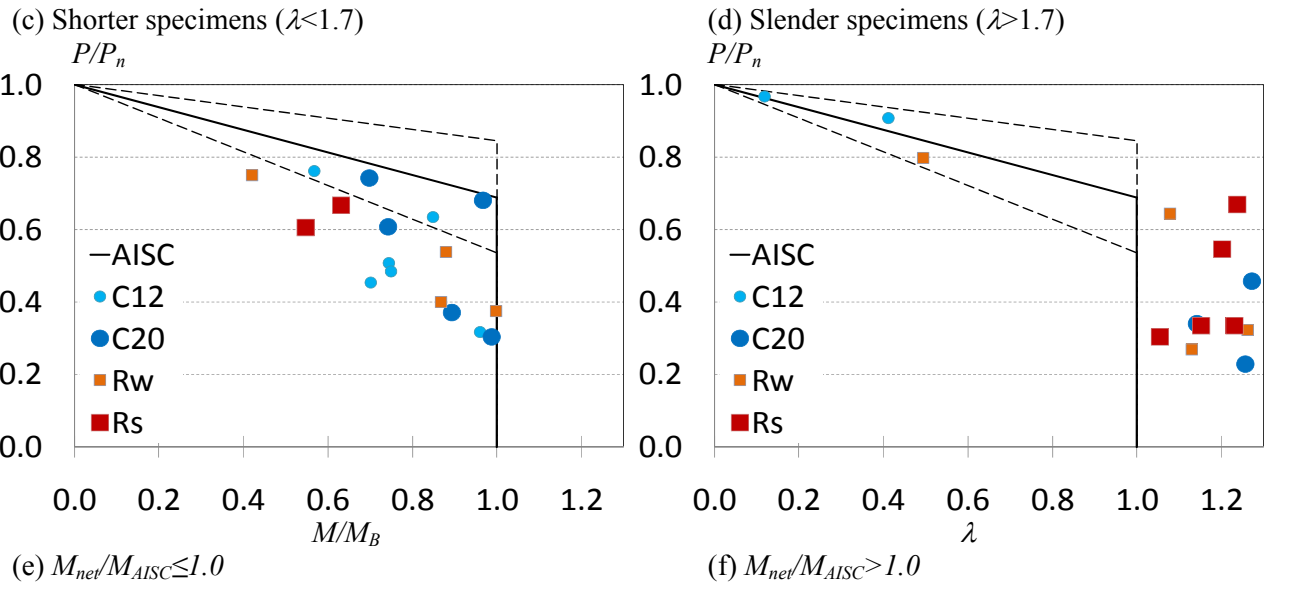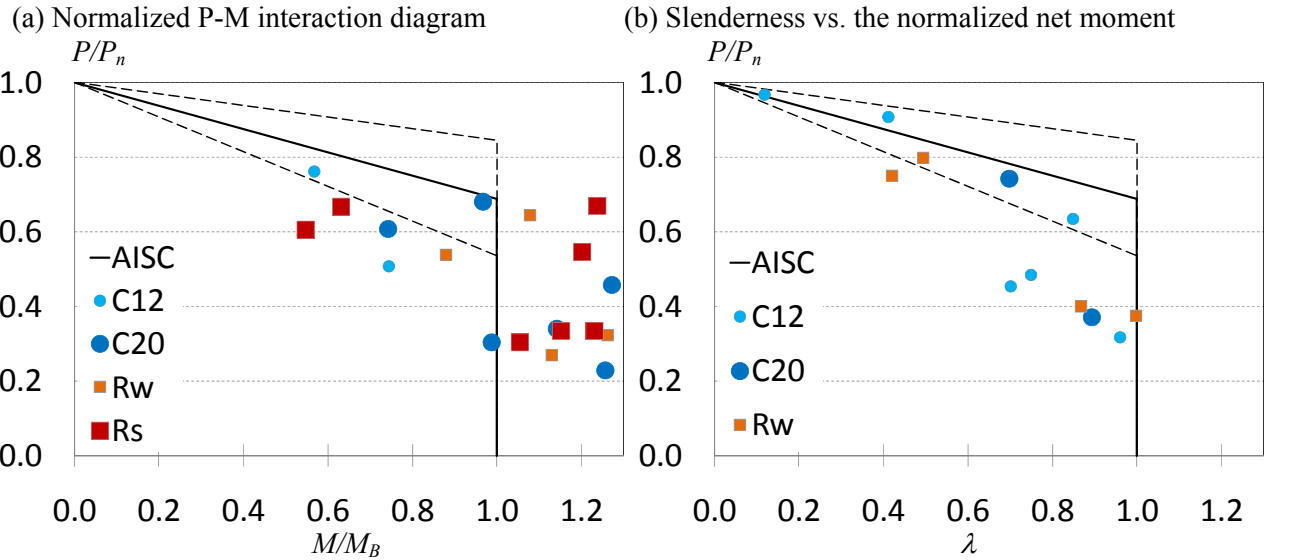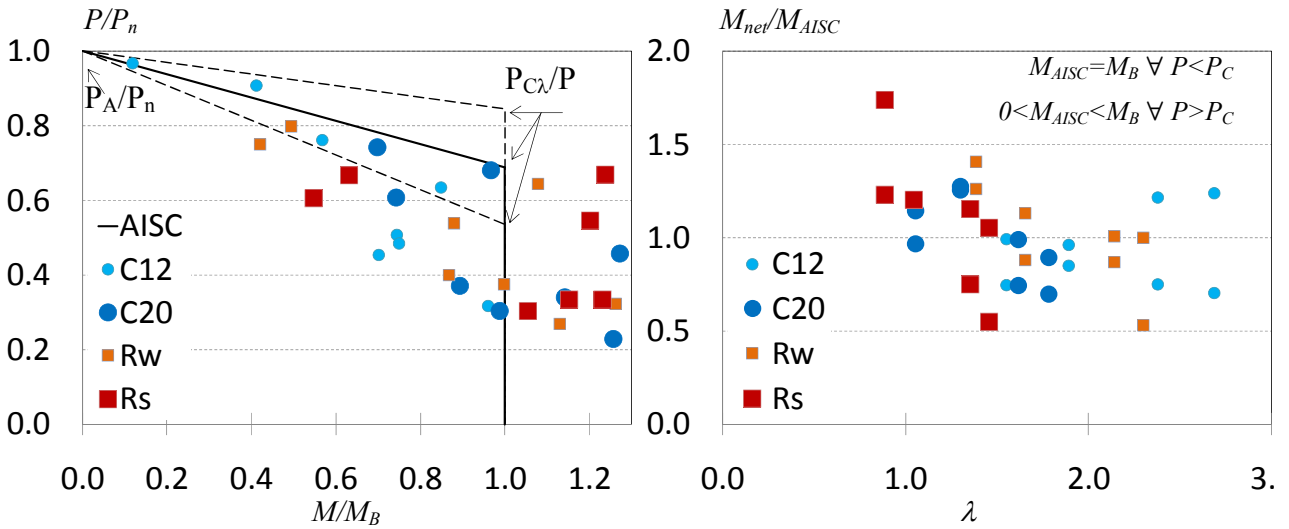
Figure 12 – Experimental net moments normalized to the AISC strength

In addition, the slenderness parameter of the column (λ) does not show proportional variation with the test data. Instead, a constant averaged coefficient of $C_3 = 0.80$ was obtained for the determination of the buckling strength of a CFT column:

$$EI_{eff} = E_s I_s + 0.80 E_c I_c \tag{4}$$
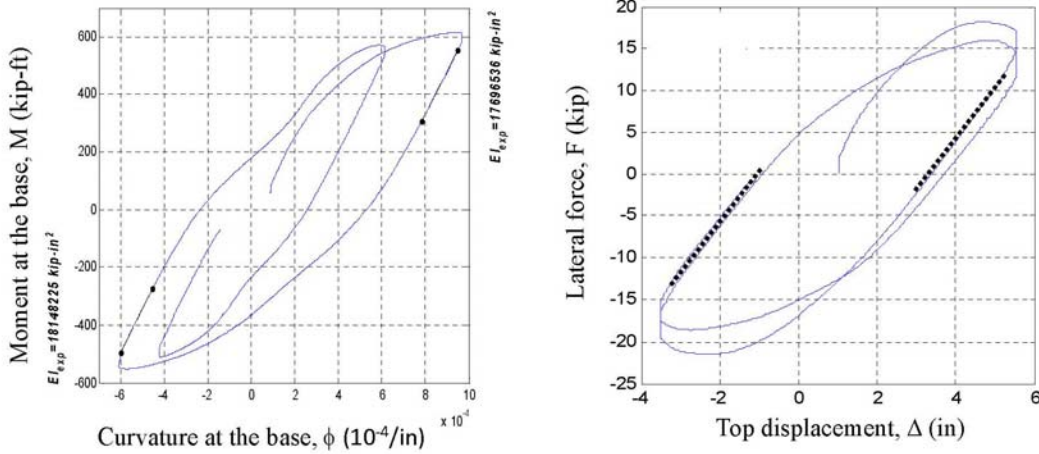
$$EI_{test} = \frac{M_b - M_a}{\phi_b - \phi_a}$$

$$\Delta = \left(\frac{FL^3}{3EI_{test}}\right)\left(\frac{1}{1 - P_{test}/P_e}\right)$$

$$EI_{test} = \left(\frac{F_b - F_a}{\Delta_b - \Delta_a}\right)\frac{L^3}{3} + \left(\frac{KL}{\pi}\right)^2 P_{test}$$

Figure 13 – Extraction of average stiffness values.

- Similarly, averaged values of the flexural rigidities were also extracted from the response during the uniaxial and biaxial loading cases (LC2 and LC3). This is a unique set of data since this intends to give a simplified equation that approaches the expected rigidity for a beam-column under seismic loading (i.e., combined constant axial load and cyclic uniaxial or biaxial lateral load). As expected, the scatter of the data increased as the damage progressed on the specimen; even with some dispersion is exhibited in the averaged test data, the following equations are proposed for the determination of the effective stiffness of a CFT beam-column under seismic loading, and for the evaluation of lateral and flexural capacity based on frame analysis.

When local buckling is not expected (as in compact cross sections)::

$$EI_{eff} = E_s I_s + 0.40 E_c I_c \tag{5}$$

On the other hand, when the steel tube is susceptible to local buckling:

$$EI_{eff} = 0.85\left(E_s I_s + 0.40 E_c I_c\right) \tag{6}$$

Steel Local Buckling in CFT Members

Extraction of the first occurrence of local buckling in the 18 specimens tested for this project was based on multiple measurements from the instrumentation (Figure 13). Based on the data extracted from these tests, an update of the current AISC empirical equations for the longitudinal strain in the steel tube at the initiation of local buckling is proposed for both CCFT and RCFTs. The proposed equations are:

For circular concrete filled tubes (CCFTs):

$$\varepsilon_{lb} = 0.09 \left(\frac{D}{t} \cdot \frac{F_y}{E_s} \right)^{-2} \frac{F_y}{E_s} = \frac{0.09}{\lambda^2 \cdot \varepsilon_y} \tag{7}$$

For rectangular concrete filled tubes (RCFTs):

$$\varepsilon_{lb} = 9 \left(\frac{h}{t} \sqrt{\frac{F_y}{E_s}} \right)^{-2} \frac{F_y}{E_s} = \frac{9}{\lambda^2} \tag{8}$$

From the empirical equations shown above, an update of limits for slender (λ_r) and non-compact (λ_p) filled tubes are proposed as follow:

For circular concrete filled tubes (CCFTs) with slender steel sections

$$\lambda_r = 0.3 \frac{E_s}{F_y} \tag{9}$$

For circular concrete filled tubes (CCFTs) with non compact steel sections

$$\lambda_p = 0.15 \frac{E_s}{F_y} \tag{10}$$

For rectangular concrete filled tubes (RCFTs) with slender steel sections

$$\lambda_r = 3.0 \sqrt{\frac{E_s}{F_y}} \tag{11}$$

For rectangular concrete filled tubes (RCFTs) with non compact steel sections

$$\lambda_p = 2.12 \sqrt{\frac{E_s}{F_y}} \tag{12}$$

Plastic Hinge Length in CFT Members

An analysis of the plastic hinge lengths was made, based on the maximum curvature within the column length, throughout the load protocol. Based on this data analysis, the equation below proposed for steel sections presents a reasonable prediction of the plastic hinge length.

$$L_p = L \left(1 - \frac{M_y}{M_p} \right) = L \left(1 - \frac{S}{Z} \right) = L \left(1 - \frac{1}{k_s} \right) \tag{13}$$

(a) CCFTs   (b) RCFTs
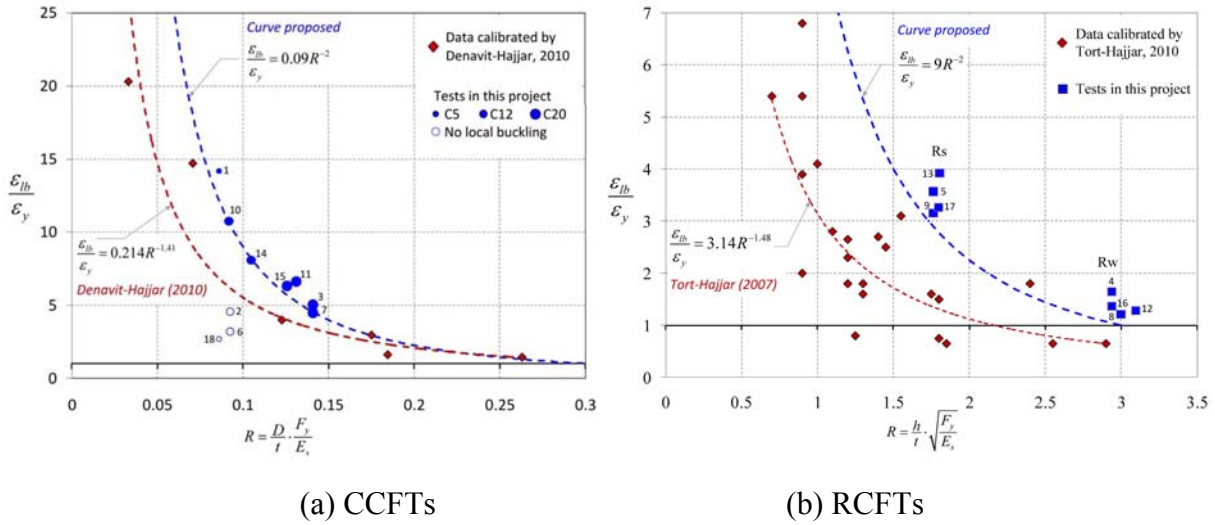
Figure 13 – Comparison between local buckling from this study and data used to calibrate current AISC Equations

Torsional Strength and Stiffness of CFT Members

The experimental torsional response obtained from the tests of the CFT specimens points out the following behavior:

- The results indicate a partial contribution of the concrete to both the torsional strength and the torsional rigidity. Both the strength and the stiffness contributions were calibrated with the test data and design equations developed for torsion.
- The strength response under torsion and combined axial load was slightly higher than the strength obtained in pure torsion only in CCFTs; due to high damage accumulation, the torsion strength with and without compression was very similar to the pure torsion strength.
- The torsional stiffness is slightly higher in CCFTs due to better performance of circular cross section shapes; and earlier local buckling damage in RCFTs, which is less severe in CCFTs.

Assuming full contribution of the steel component and partial contribution of the concrete component, design equations are proposed to estimate both the torsional strength strength and the torsional rigidity for non-cyclic and cyclic loading. These design equations predict reasonable values of the torsion strength and torsion rigidity. The equations are as follows:

$$T_n = T_s + \frac{1}{4}T_c \tag{14}$$

$$GJ_{eff} = \begin{cases} GJ_s + \dfrac{1}{2}GJ_c & \text{for CCFTs} \\[2mm] GJ_s + \dfrac{1}{6}GJ_c & \text{for RCFTs} \end{cases} \tag{15}$$

VI. Analytical Studies

Evolution of Interaction Strength

The change in size, shape, and location of the beam-column interaction surface with the progression of cyclic loading was investigated. One specimen, 9Rs-18-12, was subjected to a unique loading history in its latter load cases that consisted of a series of "probes" and "subprobes". After the completion of the first three load cases, the specimen was moved to zero displacement and a compressive axial load of 3,560 kN (800 kips), which was held constant for the remainder of the test, was applied. A probe was completed by increasing the lateral displacements with a fixed ratio of X to Y displacement until a desired displacement past the limit surface was reached (stability was maintained because the lateral degrees-of-freedom were in displacement control). From this position a series of subprobes were completed by increasing the displacements in a different fixed ratio of X to Y displacement until the critical flexural strength was reached, at which point the lateral displacements were reversed to the termination point of the original probe. The process was then repeated for several additional X/Y displacement combinations. This scan about the termination point of the probe determines the current limit surface of the beam-column. The process was repeated six times, obtaining information about the interaction surface at six different points during the loading. The resulting interaction diagrams are shown in Figure 13, where each diagram represent a slice of the three-dimensional (P-$M_{x,base}$-$M_{y,base}$) interaction surface at constant the applied axial load. This behavior could significantly impact the accuracy of common nonlinear frame analysis approaches such as stress-resultant plasticity models that do not account for changes in the limit surface.
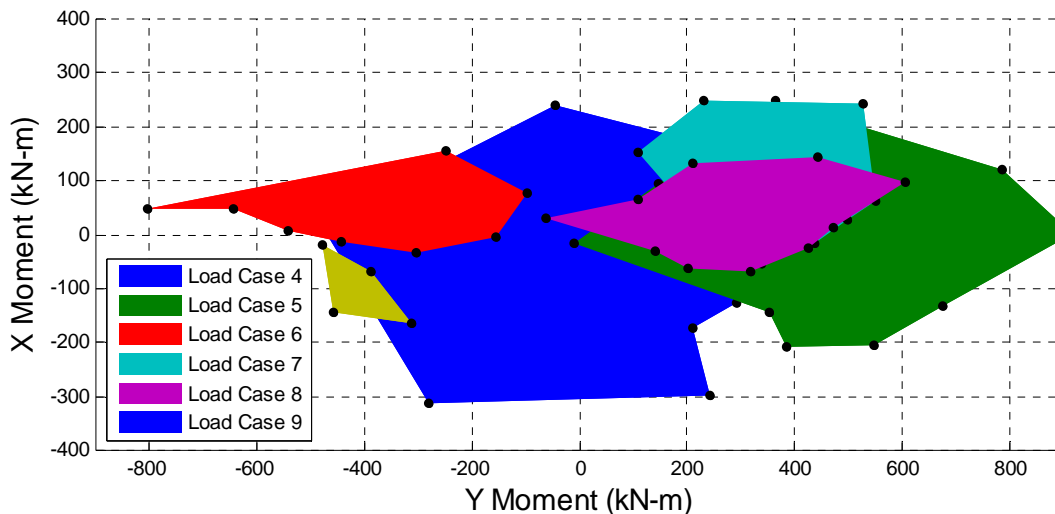
Figure 14 – Experimental Interaction Surfaces, Specimen 9-Rs-18-12

VII. *Analytical Studies*

The primary focus of the analytical research has been the development of accurate nonlinear models for the analysis of composite structures. The new formulations will enable future researchers to conduct studies including large-scale parametric investigation of composite frame systems subjected to seismic and non-seismic loading, as well as, documentation of behavioral response suitable for performance-based design provisions. Additional complementary aspects of the analytical work have included experimental database development, archetype frame design, and assessment of bond strength.

Database Development

A detailed database of experimental results of rectangular CFTs, circular CFTs, and SRCs suitable for the calibration and validation of nonlinear finite element formulations has been created. Tests with a broad range of material and geometric characteristics have been sought so that the unique characteristics of composite beam-columns can be integrated into the formulations. These models account for key characteristics such as, in the steel, gradual reduction of modulus, gradual reduction of the elastic zone, ratcheting, overshooting, and softening due to local buckling; and in the concrete, nonlinear response up until the peak stress, variation in the peak stress with confinement, post-peak softening, post-peak ductility due to confinement, tension stiffening, and crack opening and closure via cycling into tension and back into compression.

A new version of a synopsis of experimental and computational studies of CFT columns, beam-columns, connections, and frames has been published (Gourley et al. 2008). This is the fourth edition of a detailed synopsis that was first published in 1993. The synopsis includes summaries of all well-documented research on CFTs in the literature, and includes extensive tables that highlight the key parameters studied in the experimental research. This work also contributed directly to the database development that established the CFT test matrix in this work.

Advanced Nonlinear Models

A comprehensive finite element formulation for the analysis of steel and concrete composite frame structures has been developed. The model is capable of accurately modeling frame systems consisting of any combination of CFT, SRC, or wide flange steel columns, wide flange steel beams, and HSS steel braces. The models are implemented in the OpenSees framework.

Two- and three-dimensional mixed distributed plasticity fiber beam elements provide the base for the model. The element stiffness and internal force was derived in the corotational frame, allowing rigid body modes of deformation to be accounted for solely in a geometric transformation. Cubic-Hermitian and linear interpolation function were used for the transverse and axial deformation fields, while linear and constant interpolation functions were used for the bending moment and axial load fields. The Green-Lagrange strain measure was adopted to define the axial strains, while curvature was assumed to be the second derivative of the transverse deformation field. The axial strain at each of the fibers in the section is determined utilizing a

kinematic assumption (i.e., initially plane sections remain plane), neglecting any slip occurring between the steel and concrete. In the mixed formulation, element compatibility and section equilibrium are satisfied with two equations beyond element equilibrium. The simultaneous solution of all three governing equations adds to the complexity of the state determination algorithm. The unbalance from the additional equations is converted to an unbalanced force at the global level and eliminated through the global solution iterations.

Different fiber cross section discretizations assigned to the element allow for the modeling of the various steel and composite members. The fiber sections are an accumulation of many instances of the steel and concrete material models in a configuration resembling the cross section of the member to be analyzed. The properties assigned to the material models are based given material properties (e.g., F_y, F_u, or f'_c), the type of section being analyzed, and the location of the material within the section. Example fiber sections are shown in Figure 15, where each circle represents a fiber and the different colors represent material models with different properties.

(a) CCFT Section

(b) RCFT Section

(c) Wide Flange Steel Section

(d) SRC Section
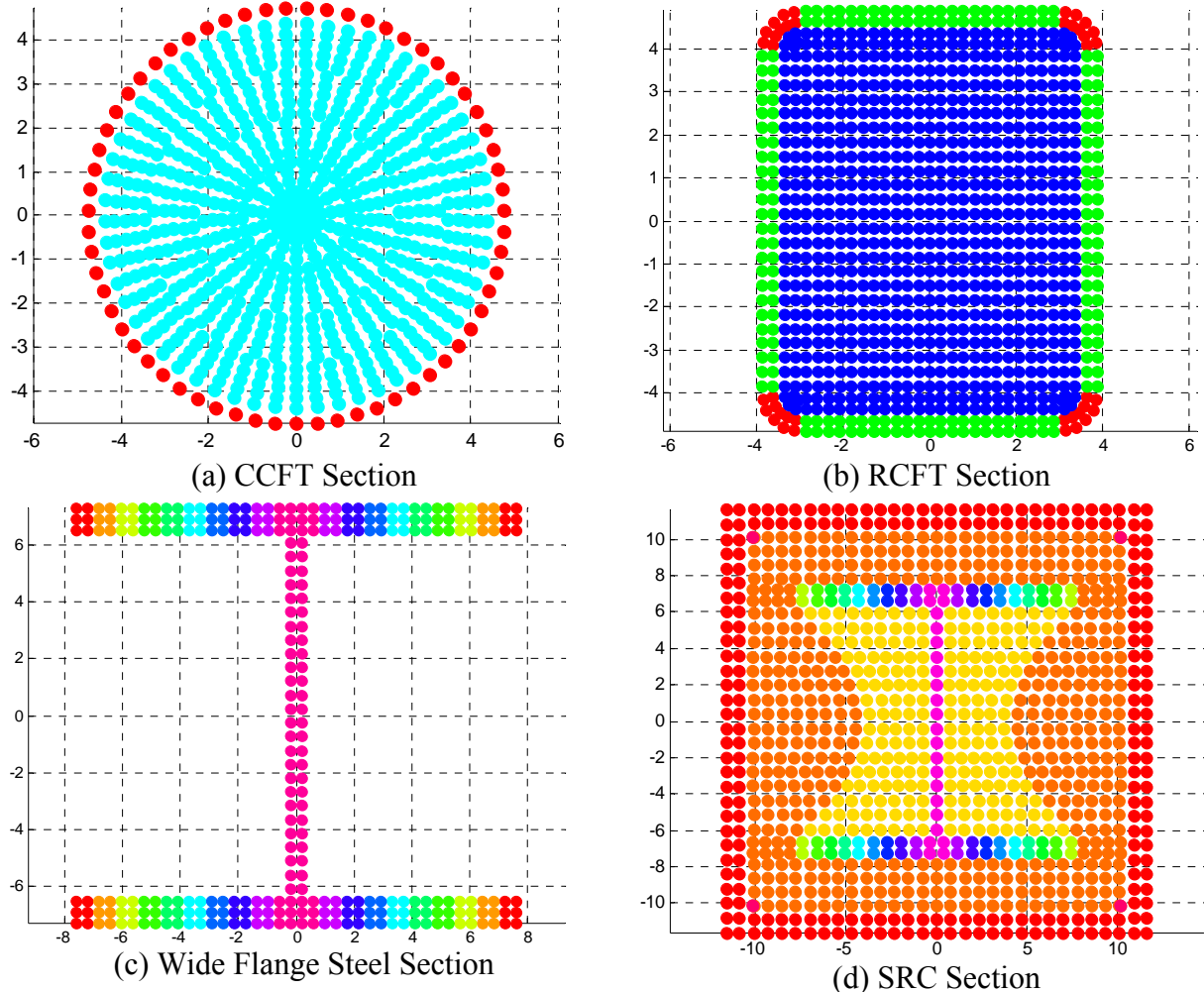
Figure 15 – Example Fiber Sections

New cyclic uniaxial material models have been implemented in the OpenSees framework. These models are based on well-established existing steel and concrete models with modifications to

allow for modeling of behavior specific to composite members. The same basic steel model and concrete model are used for all of the different sections, however, different parameters and different options built into the models, the variety of behavior observed in steel and composite members is capable of being modeled.

The steel model is based on the bounding-surface plasticity model of Shen et al. (1995). In this model, the incremental relation between stress and strain is established based on a set of hardening and flow rules. The cyclic characteristics of steel, such as strain hardening, elastic unloading, decreasing elastic zone and gradual stiffness reduction as a result of cyclic loading, Bauschinger effect, bounding stiffness, ratcheting, are represented by introducing internal variables and incorporating them with the constitutive relations. Additional characteristics were desired and thus, the following modifications were made:

- To model the built-in residual stress from cold-forming of steel tubes, an option was implemented to eliminate the yield plateau and include an initial plastic strain. This initial plastic strain can be obtained through comparisons with tensile coupon tests of cold-formed steel tubes. Initial plastic strain values of 0.0006 for CCFT members and 0.0006 and 0.0004 for the corner and flat regions, respectively, of RCFT members are found to produce accurate results.
- To model the built-in residual stress from hot-rolling of steel wide flange shapes, an option was implemented to define an initial stress. The value initial stress varies throughout the cross section so it is necessary to define multiple materials with different values of initial stress (e.g. Figure 15c).
- To model local buckling in the steel tube or the flange or web of a wide flange steel shape several optional modifications were made to the compression region of the steel model. When active, local buckling is assumed to initiate when a certain critical strain, ε_{lb}, has been reached. For strains higher than the local buckling strain, the response is assumed to be a linear descending branch, with slope K_s, followed by a constant residual stress branch, with stress F_{res}.

The constitutive relations for the concrete core are adapted from the rule-based model of Chang and Mander (1994). The stress-strain behavior is modeled with a family of close form equations in terms of strain and a set of rules which identifies the proper equation to be used for any arbitrary strain increment. Multiaxial stress conditions are accounted for implicitly by selecting the peak stress and strain at peak stress that reflect the level of confinement. It allows for comprehensive modeling of cyclic softening, cycling into tension and then back into compression, and other complex concrete phenomena.

The level of confinement experienced by the concrete has a significant impact on the behavior of CFT members. For circular members the confinement serves to increase both the strength and ductility of the concrete core, whereas, for rectangular members only the ductility is affected. The compressive backbone stress-strain curve for the concrete is based on the model of Tsai, which is defined by the initial slope E_c, peak coordinate ($\varepsilon'_{cc}, f'_{cc}$), and r factor. The initial slope and strain at peak stress for unconfined concrete, ε'_c, are defined using expressions from the literature. The peak stress and strain at peak stress are taken as the unconfined values for RCFT members, whereas for CCFT members they are computed using a confinement model and an

estimation of the confinement pressure. The r factor, which controls the nonlinear descending branch, was calibrated to the post-peak behavior of short concentrically loaded CFT columns, and also differs between CCFTs and RCFTs. These parameters were calibrated to a set of well-documented experiments on concentrically load short columns. These tests were selected to have combinations of high and low values of steel yield stress, F_y, concrete compressive strength, f'_c, and ratio of steel tube diameter or depth the thickness, D/t ratio.

The wide flange steel sections utilize only the steel uniaxial material model. The same material properties are used throughout the section, but the initial stress and local buckling behavior vary. Initial stress is defined based on the Lehigh residual stress pattern (Galambos and Ketter 1959). Local bucking of the flange has been calibrated to experimental tests.

The SRC model incorporates the wide flange model as described above; with the exception that local buckling is inhibited by the concrete section that surrounds it. The concrete is separated into three regions based on confinement (Figure 15d). The cover concrete, which lies outside the lateral reinforcing, is assumed to have zero confinement and is capable of spalling. The concrete within the lateral reinforcing is labeled moderately confined. An enhancement in strength and ductility is computed based on the confinement pressure provided by the lateral reinforcement. Additional enhancement in strength and ductility is computed for the highly confined concrete within the flanges of the steel shape.

Extensive verification studies have been performed to verify the accuracy of the model (Denavit et al. 2010). The formulation was verified against a wide range of monotonic and cyclic experiments, including short columns, beams, and proportionally and non-proportionally loaded beams columns. Several elastic and dynamic problems were also analyzed to validate the geometrically nonlinear and dynamic formulation. The studies showed that accurate results can be obtained for composite members and frames subjected to a variety of loading conditions. Figure 16a shows verification results for cyclic pure bending of circular concrete-filled steel tubes and Figure 16b shows verification results for cyclic non-proportional loading of steel reinforced concrete cantilever columns. These results show the ability of the model to capture the initial stiffness, peak strength, and unloading stiffness, the CFT also show the ability of the model to capture local buckling of the steel tube.

D = 110 mm; t = 1.25 mm; D/t = 88.0
f'_c = 23.1 MPa; F_y = 430 Mpa; L = 800 mm

D = 89.3 mm; t = 2.52 mm; D/t = 35.4
f'_c = 23.1 MPa; F_y = 378 Mpa; L = 800 mm
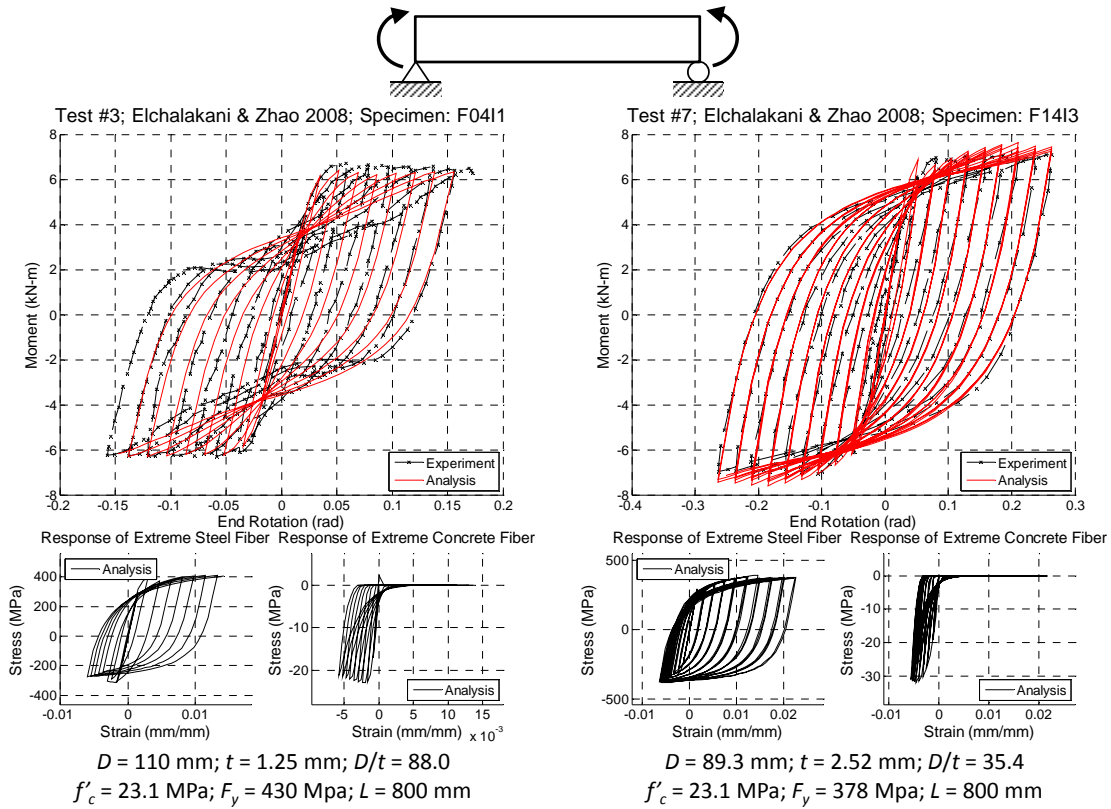
(a) Cyclic Pure Bending of Circular Concrete-Filled Steel Tubes
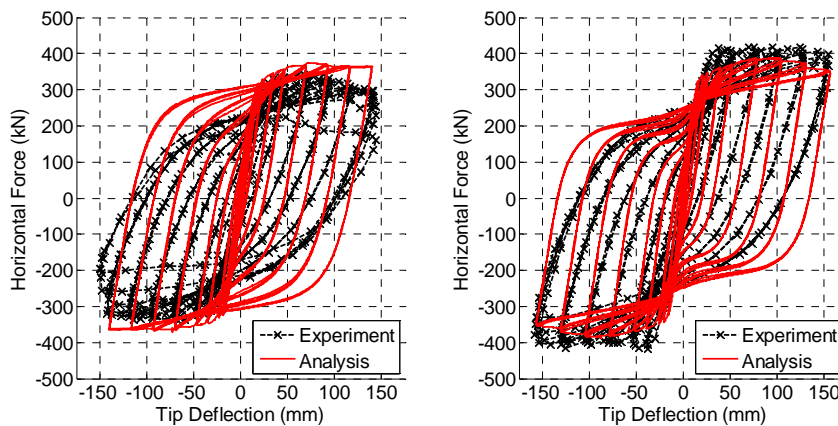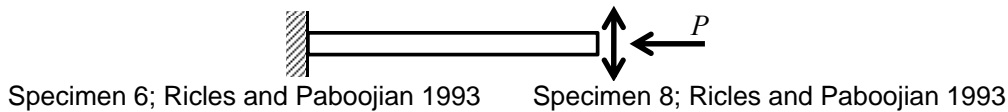
Spec-imen	H (mm)	B (mm)	f'c (MPa)	Steel Section	Fy (MPa)	db (mm)	Fyr (MPa)	L (mm)	P (kN)
6	406	406	35.8	W 8x40	372	28.6	448	1,930	1,490
8	406	406	62.9	W 8x40	372	22.2	434	1,930	1,490

(b) Cyclic Non-Proportional Loading of Steel Reinforced Concrete Cantilever Columns

Figure 16 – Cyclic Verification Results

This formulation has been successful in capturing the behavior exhibited by the specimens tested the MAST facility even in the more complex three-dimensional load cases. Figure 17 shows a comparison of results for specimen 11 in load case 3a.
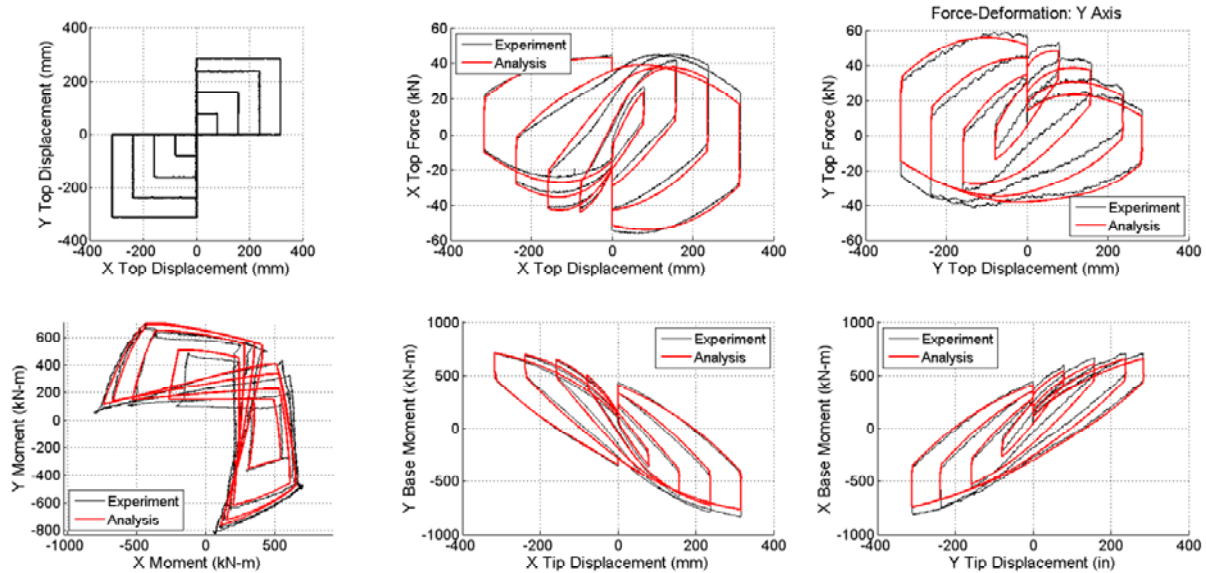
Figure 17 – Verification Results for Specimen 11C20-26-5 – Load Case 3a

In addition to validation of the model, comparisons have been made to displacement-based and force-based beam elements using uniaxial material models based on constitutive relations from the literature. The results of these comparisons have shown that especially for the latter load cases, the current model is better capable of predicting this behavior than the existing models.

Archetype Frame Design

A complete set of twenty archetype structures have been designed using RCFT and CCFT beam-columns and steel girders and braces, ranging in height from three to eighteen stories, including both braced and unbraced frames. Parameters of the frames are shown in Table 4. These frames were selected and designed in accordance with FEMA P695 and are intended to be used for large scale parametric-studies to assess the system behavior factors (e.g., R, Cd, Ωo) for composite braced and unbraced frames and to aid in enhancing the non-seismic and seismic design provisions for these systems.

Table 4 – Archetype Frames

Frame	Lateral Force Resisting System	Column Type	Stories	Gravity Loading	Bay Width (ft)	Seismic Design Category
A1	C-SMF	RCFT[†]	3	Interior/Warehouse	20	D_{max}
A2	C-SMF	RCFT[‡]	3	Interior/Warehouse	20	D_{max}
A3	C-SMF	RCFT	3	Perimeter/Office	20	D_{max}
A4	C-SMF	RCFT	3	Interior/Warehouse	20	D_{min}
A5	C-SMF	RCFT	3	Perimeter/Office	20	D_{min}
A6	C-SMF	RCFT	3	Perimeter/Office	30	D_{max}
A7	C-SMF	RCFT	3	Interior/Warehouse	30	D_{max}
A8	C-SMF	RCFT	9	Interior/Warehouse	20	D_{max}
A9	C-SMF	RCFT	9	Perimeter/Office	20	D_{max}
A10	C-SMF	RCFT	18	Interior/Warehouse	20	D_{max}
A11	C-SMF	RCFT	18	Perimeter/Office	20	D_{max}
B1	C-SCBF	CCFT[†]	3	Interior/Warehouse	20	D_{max}
B2	C-SCBF	CCFT[‡]	3	Interior/Warehouse	20	D_{max}
B3	C-SCBF	CCFT	3	Perimeter/Office	20	D_{max}
B4	C-SCBF	CCFT	3	Interior/Warehouse	20	D_{min}
B5	C-SCBF	CCFT	3	Perimeter/Office	20	D_{min}
B6	C-SCBF	CCFT	3	Perimeter/Office	30	D_{max}
B7	C-SCBF	CCFT	3	Interior/Warehouse	30	D_{max}
B8	C-SCBF	CCFT	9	Interior/Warehouse	20	D_{max}
B9	C-SCBF	CCFT	9	Perimeter/Office	20	D_{max}

[†]CFT members designed with lower D/t ratio, [‡]CFT members designed with higher D/t ratio

Bond Strength for CFT Columns

Work has been completed to improve the assessment of the bond strength of CFTs. A new approach for assessing the nominal bond strength for both rectangular and circular concrete-filled steel tubes (CFT) has been proposed. Based on comparisons to push-out test of concrete-filled steel tubes, an equation was developed to compute the nominal bond stress as a function of tube dimensions. This equation is conservative, in that it neglects experiments in which the load is introduced via shear tabs, which exhibit small rotations and bear against the concrete, thus increasing the bond stress; future research will investigate incorporation of these tests. The longitudinal bond transfer length was derived by examining the distribution of bond stress along the height of the column as well as experimental data from CFT connection tests. The circumferential bond transfer width was identified for CFTs as the entire perimeter of the interface, accounting for the bond contribution from the interface on the sides that do not have girders or braces framing in.

The current design provisions (AISC 2005, 2010) are thus found to be conservative for most of the cases examined (except for very large diameter tubes). A new formula for nominal bond strength of CFT structures is proposed as:

$$R_n = pDC_{in}F_{in} \tag{16}$$

where

p = entire perimeter of the steel-concrete interface

D = diameter or width of the steel tube

C_{in} = 2 if the CFT extends to one side of the point of force transfer

= 4 if the CFT extends to both sides of the point of force transfer

F_{in} = bond stress

= 12100 (t/D^2) for RCFT (units: lbs, inches)

= 30600 (t/D^2) for CCFT (units: lbs, inches)

For implementation in design provisions, both minimum and maximum caps on the bond stress should be considered.

One-dimensional analyses, assuming uniform behavior around the perimeter of the interface, were performed to assess the nonlinear distribution of bond and justify the use of a uniform bond stress in design calculations. The steel tube and concrete core are modeled with truss elements and the interface is modeled with zero length springs located at the nodes. The uniaxial steel and concrete material models described above were used for the steel tube and concrete core. A bilinear, elastic-perfectly plastic model is used to describe the load-slip relationship. The results including section force distribution, slip, and bond stress along the length of the column for one of these analyses is shown in Figure 18.
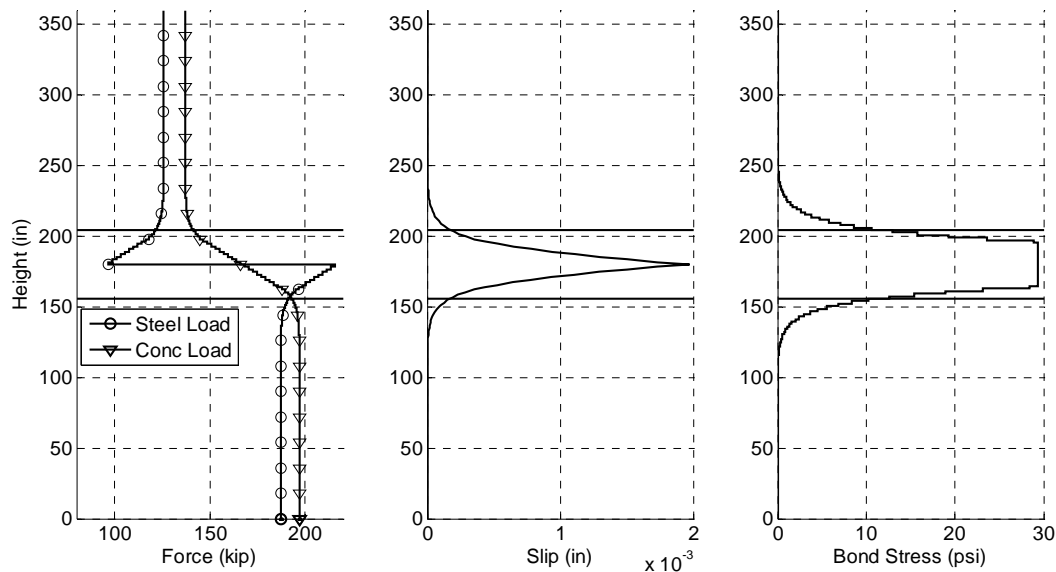
Figure 18 – Results of Bond Analysis at Design Bond Strength

VIII. *Future Work*

The experimental and analytical work completed as part of this project has made possible a wide variety of possible future studies that will further advance the knowledge of behavior of steel and concrete composite frame systems. These studies include:

- Development of direct analysis recommendations for stability design of composite frames. Direct analysis recommendations can be developed and validated against computational results from the static analyses of small sensitive benchmark frames.
- Development of equivalent stiffness recommendations for elastic analyses of composite frames. Equivalent stiffness values for composite columns are used in elastic analyses to determine the fundamental frequencies of vibration of a structure, as well as seismic force and deformation demands. Such recommendations should account for the effect of material nonlinearity, most notable concrete cracking, on the average frame behavior. Recommendations could be developed through comparisons between computational results from static and dynamic analyses of the archetype frames and elastic frame analyses utilizing equivalent stiffness values.
- Development of seismic performance factors for composite special moment resisting frame and composite special concentrically braced frame systems. A methodology has been developed recently for the development of seismic performance factors (FEMA 2009). The methodology has a strong dependence on the nonlinear static and dynamic analyses. Static pushover analyses are used to determine the system overstrength factor (Ω_o), while incremental dynamic analyses are used to determine the response modification factor and the deflection amplification factor (R and C_d).
- Investigation of seismic stability for composite frames. Prior research has indicated that the direct analysis method has limited applicability for seismic design. Stability issues relevant to the seismic performance of composite frames could be studied utilizing fully nonlinear frame analyses as a point of comparison.
- Refinement of proposed bond strength equations to account for additional experiments that include loading on shear-tabs to induce slip in CFTs.

IX. *Design Recommendations*

As a result of the experimental and analytical studies reported herein, a number of proposals will be made to AISC TC5 for the 2015 code cycle. Beyond the proposals for provisions for wet concrete forces, local buckling and torsional forces described above, new interaction equations will be proposed. These take the form shown in Tables 5 and 6 for the determination of the P-M interaction diagram of CFT cross-sections. For simplicity, the plastic stress distribution method was adopted in the derivations of the cross-section strength; however, If desired or possible, the cross-section strength obtained in this simplified fashion can be replaced by the more exact capacity obtained with the strain compatibility method.

A proposed methodology for the determination of the $P\text{-}M_\lambda$ interaction diagram of CFT beam-columns is illustrated in Figure 19, where the beam-column capacity is obtained as the cross-section strength reduced by the lost capacity due to stability and imperfection effects.

Table 5 – Equations for the P-M interaction diagram of RCFT cross-sections

Geometric properties:

$$h_c = h - 2t$$

$$b_c = b - 2t$$

$$r_s \approx 2t$$

$$r_c = r_s - t = t$$

$$A_c = b_c h_c - (4-\pi) r_c^2 = b_c h_c - 0.8584 t^2$$

$$A_s = bh - (4-\pi) r_s^2 - A_c = bh - b_c h_c - 2.5752 t^2$$

$$Z_c = \frac{b_c h_c^2}{4}$$

$$Z_s = \frac{bh^2}{4} - Z_c$$

$$I_c = \frac{b_c h_c^3}{12}$$

$$I_s = \frac{bh^3}{12} - I_c$$

Material properties:

$$F_c = 0.85 f_c{}'$$

Anchor points:

$$P_s = A_s F_y \qquad P_c = A_c F_c$$

$$P_o = P_s + P_c \qquad T_o = -P_s$$

$$P_b = \frac{P_c}{2} \qquad M_b = Z_s F_y + \frac{1}{2} Z_c F_c$$

$$M_o = M_{cs}(y_o) \qquad y_o = \frac{P_c/2}{4tF_y + b_c F_c}$$

$$M_o = M(y_o) \quad ; \quad P(y_o) = 0$$

P-M continuous functions:

$$\forall \quad -\frac{h_c}{2} < y < \frac{h_c}{2}$$

$$P(y) = \left(\frac{h_c}{2} - y\right) b_c F_c - 4ytF_y$$

$$Z_c(y) = Z_c - b_c y^2$$
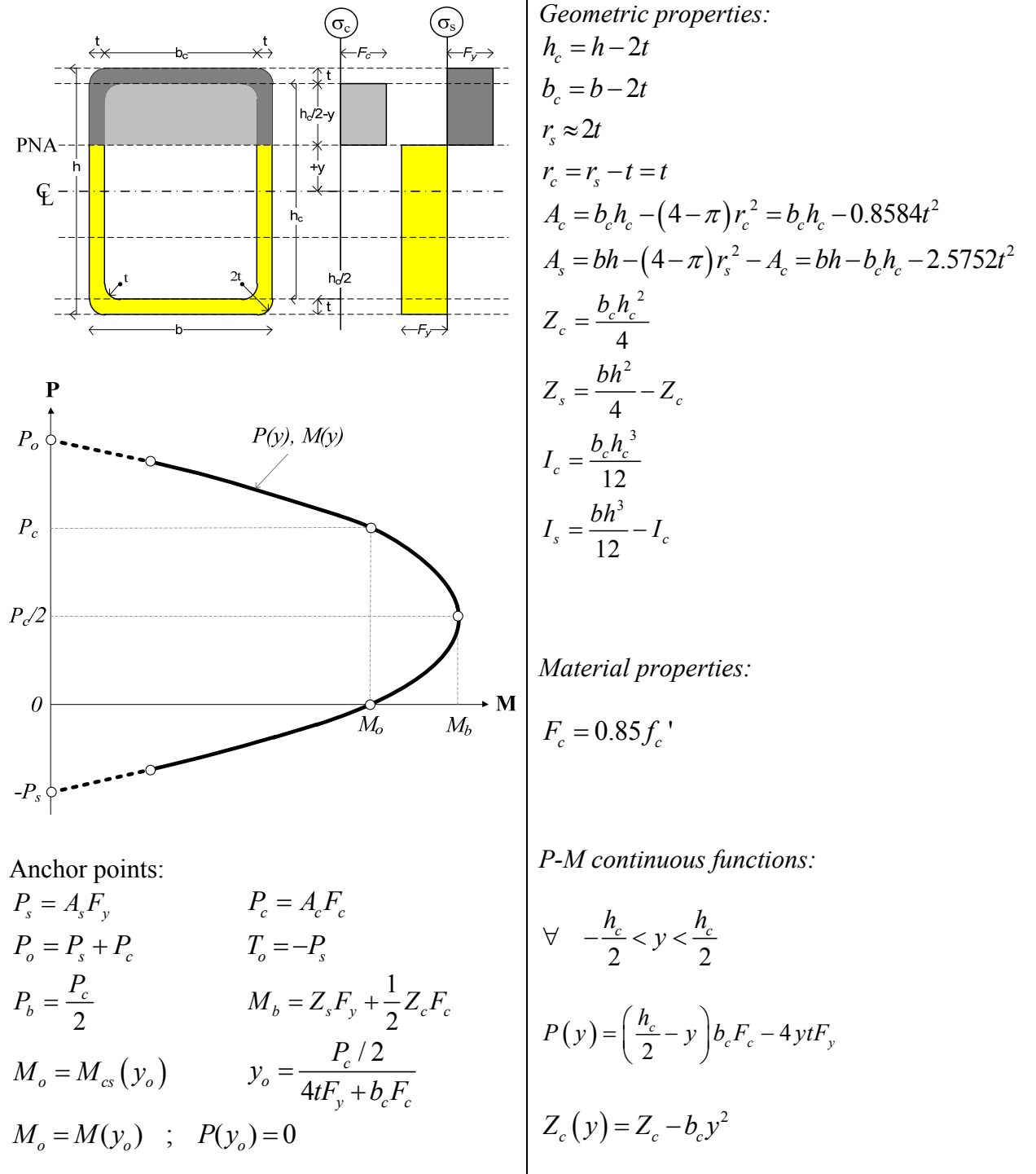
$M_o = M(-y_o)$; $P(-y_o) = P_c$ $y_i = \dfrac{P_c/2 - P_i}{4tF_y + b_cF_c}$ $\qquad y_n = \dfrac{P_c/2 - P_n}{4tF_y + b_cF_c}$ $M_n = M(y_n)$; $P(y_n) = P_n$	$Z_s(y) = Z_s - 2ty^2$ $M(y) = Z_s(y)F_y + \dfrac{1}{2}Z_c(y)F_c$

Table 6 – Equations for the P-M interaction diagram of CCFT cross-sections

Geometric properties:

$$D_c = D - 2t \qquad\qquad A_c = \frac{\pi D_c^2}{4}$$

$$A_s = \pi D^2/4 - A_c \qquad \text{or} \qquad A_s = \pi(D-t)t$$

$$Z_c = \frac{D^3}{6} \qquad\qquad Z_s = \frac{D^3}{6} - Z_c$$

$$I_c = \frac{\pi D_c^4}{64} \qquad\qquad I_s = \frac{\pi D^4}{64} - I_c$$

Material properties:

$$F_c = 0.85 f_{cc} = 0.85\left(f_c' + \frac{1.558 F_y t}{D_c}\right) \qquad \text{or}$$

$$F_c = 0.85 f_c'\left(-1.254 + 2.254\sqrt{1 + \frac{7.94 f_l}{f_c'}} - 2\frac{f_l}{f_c'}\right)$$

$$f_l = \left(0.138 - 0.00174\frac{D}{t}\right)\frac{2F_y}{D/t - 2} \geq 0$$

$$K_c = \frac{D_c^2}{8}F_c \qquad\qquad K_s = \frac{D^2 - D_c^2}{2}F_y$$

P-M continuous functions:

$$\forall \quad -\frac{D_c}{2} < y < \frac{D_c}{2}$$

$$\theta(y) = 2\cos^{-1}\left(\frac{2y}{D_c}\right)$$

$$P(y) = (\theta(y) - \pi)K_s + (\theta(y) - \sin\theta(y))K_c$$

Anchor points:

$$P_s = A_s F_y \qquad\qquad P_c = A_c F_c$$

$$P_o = P_s + P_c \qquad\qquad T_o = -P_s$$

$$P_b = \frac{P_c}{2} \qquad\qquad M_b = Z_s F_y + \frac{1}{2}Z_c F_c$$

$$M_o = M_{cs}(y_o) \qquad\qquad y_o = \frac{D_c}{2}\cos\left(\frac{\theta_o}{2}\right)$$

$$\theta_o \approx \frac{0.2K_c - K_s}{0.68K_c} + \sqrt{\frac{(0.2K_c + K_s)^2 + 3.4K_cK_s}{0.68K_c}}$$

$\theta_o \approx 2\sec^{-1}\sqrt{\dfrac{K_s}{K_c}+1}$ or $\theta_o \approx \left(\dfrac{5\pi K_s}{K_c}\right)^{1/4}$	$Z_c(y) = Z_c \sin\left(\dfrac{\theta}{2}\right)^3$
$M_o = M(y_o)$; $P(y_o) = 0$	$Z_s(y) = Z_s \sin\left(\dfrac{\theta}{2}\right)$
$M_o = M(-y_o)$; $P(-y_o) = P_c$	
$M_n = M(y_n)$; $P(y_n) = P_n$	$M(y) = Z_s(y)F_y + \dfrac{1}{2}Z_c(y)F_c$
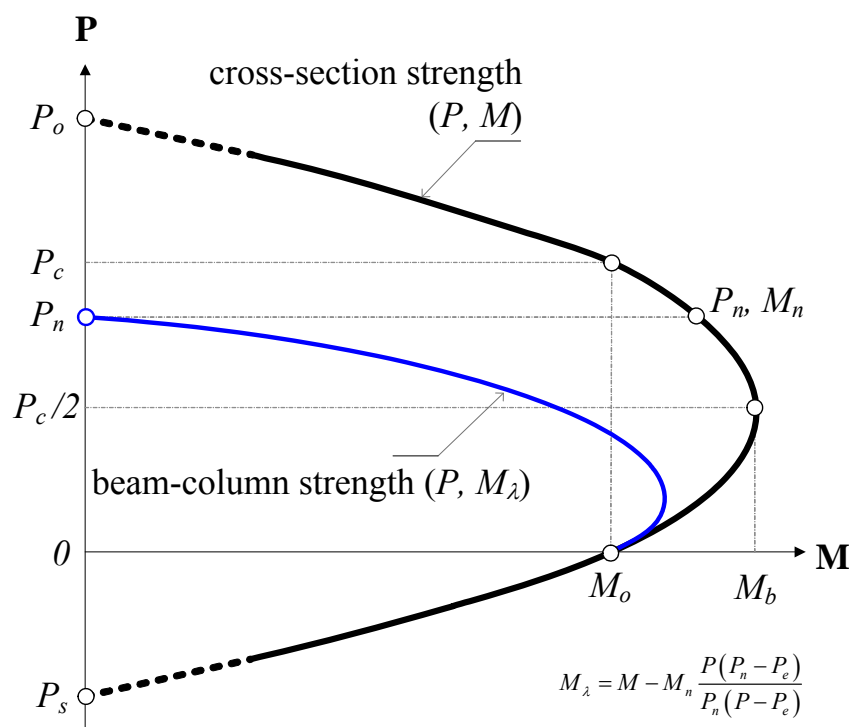
Figure 19 – Determination of the P-M_λ interaction diagram of CFT beam-columns accounting the reduction by stability and imperfections to the cross-section strength.

$$M_\lambda = M - M_n\frac{P(P_n - P_e)}{P_n(P - P_e)}$$

Acknowledgements

References

American Institute of Steel Construction (AISC) (2005). ANSI/AISC360-05: *Specification for Structural Steel Buildings*, AISC, Chicago, Illinois.

American Institute of Steel Construction (AISC) (2010). ANSI/AISC360-10: *Specification for Structural Steel Buildings*, AISC, Chicago, Illinois.

Chang, G. A. and Mander, J. B. (1994). "Seismic Energy Based Fatigue Damage Analysis of Bridge Columns: Part I - Evaluation of Seismic Capacity," Report No. NCEER-94-0006, National Center for Earthquake Engineering Research, State University of New York, Buffalo, NY.

Denavit, M. D., Hajjar, J. F., Perea, T., and Leon, R. T. (2010). "Cyclic evolution of damage and beam-column interaction strength of concrete-filled steel tube beam-columns", 9th US National and 10th Canadian Conference on Earthquake Engineering, Toronto, Canada.

Denavit, M. D. and Hajjar, J. F. (2010). "Nonlinear seismic analysis of circular concrete-filled steel tube members and frames", Report No. NSEL-023, Newmark Structural Laboratory Report Series (ISSN 1940-9826), Department of Civil and Environmental Engineering, University of Illinois at Urbana-Champaign, Urbana, Illinois.

FEMA (2009). "Quantification of Building Seismic Performance Factors," FEMA P695, Federal Emergency Management Agency, Washington, D.C.

Galambos, T. V., and Ketter, R. L. (1959). "Columns under combined bending and thrust," *Journal of Engineering Mechanics Division*, ASCE, Vol 82, No. 2, pp. 135-152.

Goode, C. D. (2007). ASCCS Database of Concrete-Filled Steel Tube Columns. ASCCS.

Gourley, B. C., Tort, C., Denavit, M. D., Schiller, P. H., and Hajjar, J. F. (2008). "A Synopsis of Studies of the Monotonic and Cyclic Behavior of Concrete-Filled Steel Tube Beam-Columns," Report No. NSEL-008, Newmark Structural Laboratory Report Series (ISSN 1940-9826), Department of Civil and Environmental Engineering, University of Illinois at Urbana-Champaign, Urbana, Illinois, April.

Hajjar, J. F., French, C. W., Schultz, A. E., Shield, C. K., Ernie, D. W., Dexter, R. J., Du, D. H., and Bergson, P. M. (2002). "A system for multi-axial subassemblage testing (MAST): initial developments", Proceedings of the American Society of Civil Engineers Structures Congress, Denver, Colorado, April 4–6, 2002, 313–314.

Kim, D. K. (2007) "A Database For Composite Columns," M.S. Thesis, School of Civil and Environmental Engineering, Georgia Institute of Technology, Atlanta, Georgia.

Leon, R. T., Aho, M. F., and Kim, D. K. (2005). A database for encased and concrete-filled columns. Georgia Institute of Technology, Atlanta, Georgia.

Leon, R., Perea, T., Hajjar, J., and Denavit, M. (2009). "Determination of buckling loads from triaxial load tests of slender concrete", 3rd International Conference on Advances in Experimental Structural Engineering, San Francisco, California.

Perea, T. (2010). "Analytical and experimental study on slender concrete-filled steel tube columns and beam-columns", Ph.D. Thesis, Georgia Institute of Technology, School of Civil and Environmental Engineering, Atlanta, Georgia.

Perea, T., Leon, R., Denavit, M., and Hajjar, J. (2010). "Experimental tests on cyclic beam-column interaction strength of concrete-filled steel tubes", 9th US National and 10th Canadian Conference on Earthquake Engineering, Toronto, Canada.

Ricles, R. and Paboojian S. D. (1993). "Seismic Performance of Composite Beam-Columns," Report No. 93-01, ATLSS Engineering Research Center, Lehigh University, Bethlehem, Pennsylvania.

Shen, C., Mamaghani, I. H. P., Mizuno, E., and Usami, T. (1995). "Cyclic Behavior of Structural Steels. II: Theory," *Journal of Engineering Mechanics*, ASCE, Vol. 121, No. 11, pp. 1165-1172.